Theoretical models for bridging timescales in polymer dynamics

2008 J. Phys.: Condens. Matter 20 033101

(http://iopscience.iop.org/0953-8984/20/3/033101)

IOP PUBLISHING JOURNAL OF PHYSICS: CONDENSED MATTER

J. Phys.: Condens. Matter **20** (2008) 033101 (24pp) doi:10.1088/0953-8984/20/03/033101

TOPICAL REVIEW

Theoretical models for bridging timescales in polymer dynamics

M G Guenza

Department of Chemistry and Institute of Theoretical Science, University of Oregon, Eugene, OR 97403, USA

Received 27 August 2007, in final form 6 November 2007
Published 17 December 2007
Online at stacks.iop.org/JPhysCM/20/033101

Abstract

The dynamics of macromolecules are characterized by the presence of several length scales and related timescales in which relevant phenomena take place. This defines the complex nature of the liquid and renders its theoretical treatment a difficult matter. The necessity of developing theoretical approaches that can describe in a comprehensive manner properties observed at many different length scales is a fundamental challenge in polymer physics.

This review paper summarizes some key problems arising from this challenge and different approaches taken so far in attempting to solve them. Theoretical models play a pivotal role in building the infrastructure that allows one to model these multiscale properties. We present methods for coarse-graining the structure of soft-matter systems, which provide effective potentials that are input to multiscale simulations. We also present methods for coarse-graining the dynamics of macromolecules in dilute solutions and in the melt state. Although much progress has already been made, obtaining comprehensive theoretical tools that are efficient and reliable in predicting complex fluid dynamics across many timescales of interest still remains an open challenge.

Contents

1. Introduction

Macromolecular liquids and solutions belong to the extended family of soft condensed matter systems, because their dynamic and mechanical properties can be strongly modified

by relatively weak external fields. This characteristic makes them desirable materials for technological applications. Biological systems take advantage of this by producing self-organized structures on multiple length scales. Through these complex structures they provide efficient transport of information and matter inside living cells. Understanding the mechanisms that rule self-organizing processes in nature could provide the knowledge needed to build efficient synthetic machines able to self-assemble and function (molecular motors) on a small (nanometer) length scale. In these systems, processes taking place on many different length scales are correlated, since the chemical nature of the macromolecule (protein) is defined at the monomer (residue) length scale, which is of the order of nanometer. This determines the global properties of the molecules, as well as their ability to aggregate, working cooperatively in an ensemble of macromolecules, to reach self-assembled structures on the large length scales, e.g. of about 10^4 nm, and dynamics on the large timescales, e.g. of the order of milliseconds. One of the challenges in understanding these kinds of physical processes is to develop theoretical approaches that correlate properties across many length scales and timescales.

From a general point of view, while only one length scale determines the physical properties of simple liquids, the nature of complex fluids is determined by the presence of several length scales, and related timescales, where processes that define their physical properties occur [1–3]. Macromolecular liquids belong to the large family of complex fluids, because even their simplest example, i.e. a melt of homopolymer chains, exhibits phenomena on a wide range of timescales. The *structure* of homopolymer liquids is fully determined when two length scales are considered, which correspond to the monomer statistical segment length, σ, and the overall polymer dimension, i.e. its radius of gyration, $R_g = \sigma(N/6)^{1/2}$, where N is the total number of monomers in the chain. Those two length scales define the pair distribution function, $g(r)$, from which all the thermodynamic properties of the liquid can be derived [4, 5]. Homopolymer *dynamics* range from fast oscillations in side chains, which are due to intramolecular connectivity constraints, to very slow relaxation of the backbone due to local energy barriers, and diffusion of the whole chain. Phenomena of intermolecular origin add even more complexity to the dynamics of homopolymer liquids, because friction and cooperative intermolecular motion can affect the time-dependent properties of the liquid across many orders of magnitude in length and in timescales.

The theoretical treatment of structure and dynamics for macromolecular liquids, increases in difficulty when the focus is on systems that can undergo phase transition, such as polymer mixtures and diblock copolymer melts. In polymer mixtures, properties depend not only on the polymer radius of gyration and monomer length scale, analogously to homopolymer liquids, but also on the length scale of concentration fluctuations, which diverges when the system approaches its spinodal decomposition temperature. The highest temperature of the two-phase region in a binary system, is the upper critical solution temperature (UCST). The monomer length scale, which defines the range of density fluctuations, becomes the relevant length scale of demixing in specific mixtures, where an opposite trend of phase separation with temperature is observed. In this case, the phase diagram is characterized by a lower critical solution temperature (LCST). This phenomenon is the so-called 'entropic demixing', where the asymmetry in the monomeric structure of the two components of the mixture frustrates the local monomeric packing in the liquid and causes an entropy-driven phase separation at high temperature.

A new, intramolecular length scale affects the properties of block copolymer liquids, namely the size of a block. Diblock copolymers are macromolecules in which a homopolymer chain of $N_A = fN$ monomers of type A is chemically bound to a second homopolymer chain of different chemical structure containing $N_B = (1-f)N$ monomers of type B, with $N = N_A + N_B$. The block size is defined by its respective radius of gyration and the spatial dimension of the block composed of A-type monomers, for example, is given by $R_{gA} = \sigma(N_A/6)^{1/2}$. Block copolymers phase separate on the length scale that corresponds to the size of a block, because intramolecular connectivity prevents complete demixing of the two chemical species.

The ensemble of length scales that rule the properties in macromolecular liquids are generically referred to as 'mesoscopic' length scales, because they are intermediate between the atomistic, microscopic, description, which depends on chemical details, and the 'bulk', macroscopic, length scale that characterizes the thermodynamic properties of the polymeric liquid. A characteristic timescale of relaxation is associated with each length scale. In general, theoretical tools to model the mesoscopic regime are in the realm of statistical mechanics, whose purpose is to establish a formal connection between the microscopic, atomistic, description of the system and its macroscopic thermodynamic properties. Non-equilibrium statistical mechanics provides the tools to bridge different levels of coarse-graining in dynamical processes [6–8].

This paper reviews some of the work performed in the area of multiscale dynamics and coarse-graining, with a focus on some specific examples. We start from the description of theoretical procedures to coarse-grain the structure of complex macromolecular fluids, which provide the effective coarse-grained potentials required to perform mesoscale simulations as well as the mean-force potentials needed as an input to theories of dynamics on the mesoscale. This section of the review starts from the simple homopolymer liquid and proceeds by including coarse-graining of polymer liquids with intramolecular and intermolecular structures of increasing complexity, such as block copolymer liquids and polymer mixtures. In the second part of the review, we discuss coarse-graining methods for the dynamics of macromolecular liquids. We present two examples: in the first, we focus on a system with the simplest intramolecular structure, a homopolymer liquid, and study the effect of intermolecular interactions on its dynamics; in the second, we focus on the fluctuation dynamics of a single protein in solution, where complex multiscale interactions are mainly of intramolecular origin. Theoretical predictions are compared with simulations and experiments to analyze the range of validity of the proposed approaches.

2. Coarse-graining and multiscale modeling in computer simulations

Formally connecting the physics of the system so as to bridge all the different length scales (and timescales) of interest is an extremely complex task. Therefore, computer simulations play a fundamental role as a source of information about these processes [9, 10]. Computer simulations typically start with a large system containing a high number of particles (to mimic the thermodynamic limit, $V \to \infty$, $n \to \infty$ and constant density $\rho = n/V$) at some fixed thermodynamics conditions. Once the interactions between the particles are known, the space-time trajectories of the particles are calculated by numerically solving the equations of motion. A well-defined number of computational steps are executed before numerical errors build up, ultimately degrading the precision of the data obtained in the computational run. Present day computer hardware limits the range of timescales that can be simulated to $O(10^{-8})$ s for a maximum number of particles of $O(10^5)$. This resolution, while perfect for simple liquids systems [11, 12], does not allow the full simulation of complex fluids, which require the investigation of a very large number of degrees of freedom.

Several factors affect the efficiency of computer simulations and much work has been devoted to minimizing their impact in order to optimize computational time. First of all, the system to be simulated has to be brought to equilibrium. Because equilibrating sufficiently large polymeric systems at realistic densities [13] requires a long computational time, new techniques have been developed to decrease this time. Recently, Theodorou, Mavrantzas and co-workers have proposed a new procedure that takes advantage of a fast computational algorithm developed for Monte Carlo simulations, which includes an ad hoc mechanism of breaking and rebinding the polymeric chains to rapidly equilibrate the chain configuration [14]. Because the conventional molecular dynamics (MD) simulation requires an equilibration time comparable to that of the actual simulation run, decreasing the time required for equilibration, significantly reduces the total computational time of the simulation. This procedure allowed Mavrantzas, Theodoru and co-workers to perform computer simulations of melts of polymer at increasing degrees of polymerization, N, and crossing over from the unentangled to the entangled regime. While computational methods, like the one just discussed, allow one to significantly extend the range of dynamics in macromolecular liquids that can be simulated, however, the timescales investigated by experiments extend even further and new strategies have to be implemented to allow a direct comparison of those data with simulations [15–22].

Because simulations build on the ergodicity of the system and the completeness of the sampling procedure, reliable statistically averaged quantities are obtained from trajectories representing the evolution in time of a large number of particles. Moreover, trajectories have to be recorded for a sufficiently long computational time to allow the system to sample all the configurational states available at the fixed thermodynamic conditions of the simulation (temperature, volume, polymer concentration). A way to overcome these problems is to develop multiscale modeling techniques that combine information obtained from a group of independent simulations performed on a hierarchy of models where the same system is represented at different levels of coarse-graining. At each level of coarse-graining, the state of the system is specified by a set of relevant variables while small length scale variables are averaged out. Less detailed, more coarse levels of description have a smaller number of variables and capture no information on scales shorter than their characteristic length scale. However, because of the reduced number of units, simulations of coarse-grained systems run faster than atomistic level simulations, enabling the investigation on a much larger length scale. Another advantage of this procedure is that, because the information on the large spatial, long timescale is provided by the mesoscale simulation, microscopic simulations can be limited in the number of particles that are monitored and in the computational time during which data are recorded. However, multiscale modeling procedures need rigorous theoretical formalisms to correlate, in a reliable and reversible manner and across the many scales of interest, information obtained at the different levels of coarse-graining.

2.1. Effective pair potentials for mesoscale simulations

To simulate a system coarse-grained at some specific length scale, it is necessary to know the effective potential that acts between the coarse-grained units. This is an effective pair potential resulting from the mapping of many-body interactions into pair interactions, through the averaging over microscopic degrees of freedom. In this process, the potential acting between microscopic units, i.e. the potential energy in the Hamiltonian of the system, reduces to an effective potential between coarse-grained units, which is a free energy in the reference system of the microscopic coordinates. The coarse-grained potential contains contributions of entropic origin due to the microscopic, averaged-out degrees of freedom and is therefore parameter dependent. For example, the effective potential acting between the centers of mass of two interacting polymers, discussed below, depends on temperature, density, degree of polymerization, and effective segment length.

Parameter-dependent effective pair potentials have to be handled with care. Because the form of the potential depends on the procedure used to derive it, different procedures can lead to different effective potentials, even for the same system. For systems characterized by density-dependent effective potentials obtained from pair distribution functions, the calculation of the equation of state has to make use of the compressibility equation, derived in the grand canonical ensemble, which includes an integral over the density. The use of the pressure (virial) or energy equations can lead to quantitative errors in the estimate of thermodynamic properties [23].

In the most common procedure, once the level of coarse-graining is defined by the selection of the effective units (e.g. the monomer, or a block, or the whole polymer for a macromolecular liquid), the potential is obtained from their pair distribution function, $g(r)$ [4, 5]. For most systems, the

potential has to be derived through a numerical, self-consistent procedure. However, for a few simple cases the procedure can be analytical, which has some advantages. Analytical potentials, which are explicitly state dependent, are convenient because they are immediately transferable across different state points.

Because the key quantity in the derivation of the potential is the pair distribution function, $g(r)$, the following section briefly summarizes the definition and the properties of this function for a simple liquid. For the complex fluids discussed in this paper, the pair distribution function has a slightly more involved formalism. However, when a polymer is mapped onto a soft colloidal particle, the description of the coarse-grained system recovers the formalism of a simple liquid, with particles interacting through the effective pair potential.

2.2. Theoretical background: the pair distribution function for simple liquids

In a uniform fluid of density $\rho = n/V$, with n the number of particles and V the volume, the structure of the fluid is fully determined by the radial distribution function, $g(r)$ with $r = |\mathbf{r} - \mathbf{r}_0|$, which is the conditional probability density of finding a particle at position $\mathbf{r}$ given that another particle is located at $\mathbf{r}_0$. In our description, particles are the effective units of the coarse-grained system. For macromolecules coarse-grained at the center of mass (com) level the formalism remains consistent to the one for simple liquids, once the particle density is defined, accordingly, as the number of polymeric chains per unit of volume. For macromolecules containing N monomers, the 'chain' density is defined as $\rho_{\mathrm{ch}} = \rho/N$.

It is often convenient to work with the total correlation function, $h(r) = g(r) - 1$, which is the difference between the distribution function and its random value of unity. The total correlation function is a function of the *direct* correlation function, $c(r)$, which was introduced by Ornstein and Zernike. For an isotropic, homogeneous liquid the Ornstein–Zernike (OZ) equation reads

$$h(r) = c(r) + \rho \int c(|\mathbf{r} - \mathbf{r}'|)h(r')\,\mathrm{d}\mathbf{r}', \tag{1}$$

where the total correlation function between two particles is given by the direct correlation function, $c(r)$, plus indirect contributions due to the propagation of the interaction through the surrounding fluid. The long-ranged effective potential between a pair of particles in the field of the surrounding ones, is given by the potential of mean force, which is a function of $h(r)$,

$$\beta w(r) = -\ln g(r) \approx -h(r), \tag{2}$$

and is long ranged, while the direct correlation function, $c(r)$, has a range comparable to that of the effective pair potential, $-\beta v(r)$. For systems with low particle density, the total and direct correlation functions become identical, as $h(r) \approx c(r) \approx -\beta v(r)$, and the mean-force potential reduces to the effective potential, $w(r) \approx v(r)$.

For homogeneous, isotropic liquids the OZ equation reduces in Fourier space to a simple algebraic equation

$$c(k) = \frac{h(k)}{1 + \rho h(k)}, \tag{3}$$

that connects two unknown functions, $c(k)$ and $h(k)$. Solving it requires coupling it with a second closure equation, which reads in real space as

$$g(r) = \exp[-\beta v(r) + h(r) - c(r) + B(r)]. \tag{4}$$

Equation (4) represents a diagrammatic expansion of $g(r)$, and it is difficult to solve because we don't know the bridge function $B(r)$. Approximated solutions of this equation entails neglecting certain classes of diagrams, which leads to the known equations, i.e. the so-called 'closure approximations'. Among those, we mention the Percus–Yevick (PY) closure, defined as

$$c(r) = g(r)[1 - \exp(\beta v(r))], \tag{5}$$

and the hypernetted chain (HNC) approximation,

$$g(r) = \exp[-\beta v(r) + h(r) - c(r)]. \tag{6}$$

The PY closure yields accurate results for systems that have a short-range, hard-core potentials, while the HNC closure is accurate for systems that have soft-core, long-range interactions [5]. Typically, monomer–monomer interactions have a strong repulsive hard-core component and are short ranged (range of the order of the monomer length scale), which supports the use of the PY closure coupled to the Ornstein–Zernike equation [24, 25]. On the other hand, when polymers are coarse-grained at the center of mass level, the potential becomes long ranged (range of the order of R_{g}) and soft, which is well represented by a HNC closure [26, 27].

Once the OZ equation is solved by coupling it with the proper closure approximation, and the effective potential, $v(r)$, is calculated, various thermodynamic quantities of interest can be derived from the pair distribution function, $g(r)$. These include the isothermal compressibility, χ_{T}, as the limit at zero wavevector of the static structure factor (compressibility equation),

$$\lim_{k\to 0} S(k) = 1 + \rho h(k) = \rho k_{\mathrm{B}} T \chi_{\mathrm{T}}, \tag{7}$$

the pressure (pressure or virial equation),

$$P = k_{\mathrm{B}} T \rho - \frac{2\pi\rho^2}{3} \int_0^\infty r^3 \frac{\mathrm{d}v(r)}{\mathrm{d}r} g(r)\,\mathrm{d}r, \tag{8}$$

and the energy that, for a liquid containing n particles, reads (energy equation)

$$U = \frac{3k_{\mathrm{B}}Tn}{2} + 2\pi n\rho \int_0^\infty r^2 v(r) g(r)\,\mathrm{d}r. \tag{9}$$

For polymers described at the microscopic, monomer level, the Ornstein–Zernike equation acquires a matricial form that requires the adoption of proper 'molecular closures' [24, 25]. There is extensive literature on this problem and the following sections will briefly discuss specific cases, as needed.

2.3. Numerical evaluation of coarse-grained potentials

Numerical procedures optimize the potential by minimizing the errors in its predictions against available simulation data. The numerical procedure starts by performing atomistic computer simulations, followed by the numerical computation of the coarse-grained pair distribution function, $g(r)$. From the latter, a first estimate of the coarse-grained potential is obtained, through the Boltzmann inversion procedure, given by the mean-force potential, $v_0(r) = w(r)$. A new simulation of the coarse-grained system interacting through $v_0(r)$, is then performed. From the simulation the coarse-grained pair distribution function is calculated, $g_1(r)$, together with its corresponding mean-force potential, which gives a new estimate of the effective potential, $v_1(r) \approx w_1(r) = -k_B T \ln g_1(r)$. By repeating this procedure, a newly estimated effective pair potential, $v_{i+1}(r)$, is obtained from the potential in the previous cycle, through the following prediction–correction method [28]

$$v_{i+1}(r) = v_i(r) + k_B T \ln \frac{g_i(r)}{g(r)}. \tag{10}$$

This procedure is repeated until convergence of the pair distribution function is achieved. Other numerical optimizations have been proposed, which have a degree of success comparable to that of the Boltzmann inversion procedure of equation (10) [29].

Determining the effective pair potential by numerically reproducing the simulated pair distribution function relies on the fact, demonstrated by Evans, that for a system described by a pairwise-additive potential there is a unique functional relationship between the pair correlation function and the potential [30]. Evans has also shown that this statement holds only in the case that the pair correlation function is known exactly and over an infinite range. Since simulations produce data that are neither exact nor infinite, the numerical evaluation of the potential is bound to carry numerical errors [28].

A general weakness of the numerical procedures is due to the fact that the pair distribution function is not very sensitive to changes in the numerical value of the potential. Different potentials, used as an input to coarse-grained simulations of identical systems, can produce pair distribution functions that are practically indistinguishable, with differences within the precision of the atomistic simulation data against which they are compared. However, small differences in the shape and value of the potential can strongly affect other properties, such as the values of thermodynamic quantities. For example, it is known that since the coarse-graining of atomistic systems produces effective potentials that are softer than the microscopic scale ones, often simulations that use numerically assessed potentials predict liquids that are too compressible.

Because the coarse-grained potential is parameter dependent, its derivation through a self-consistent numerical optimization suffers from the drawback of requiring that an atomistic simulation has to be performed for each set of initial conditions of interest. The number of parameters entering the potential can be high, and its systematic numerical derivation for each set of coupled parameters can rapidly become computationally prohibitive. As an example, we mention that the effective potential for a liquid of macromolecules depends not only on thermodynamic parameters, such as temperature, T, and total site density, ρ, but also on molecular parameters, such as local flexibility and degree of polymerization, N. When liquids of diblock copolymers are investigated, the effective potential depends also on chain composition, f, and the interaction parameter $N\chi_{\text{eff}} \propto T^{-1}$, where χ_{eff} defines the proximity of the system to its order–disorder transition [31]. For mixtures of macromolecules, thermodynamic parameters include also the polymer volume fraction, as well as their χ_{eff} parameter. In practice, numerical potentials are often used for state points that are close enough to the one for which the potential was parametrized, and in that range the potential is assumed to be state independent, so that transferability is not a problem. However, in this case, the range of applicability of the potential is strongly limited.

Finally, when the coarse-grained potential is calculated numerically from microscopic simulations, those have to be performed for length scales and timescales large enough to ensure a reliable numerical predictions of the potential at the length scale characteristic of the coarse-graining procedure, which strongly limits the computational gain of adopting a coarse-graining procedure.

In conclusion, the numerical derivation of a coarse-grained potential from microscopic simulations partially defeats the purpose of adopting a coarse-graining procedure, because it requires long-time, large-scale microscopic simulations to be performed for each set of parameters of interest. As a consequence, it is often the case that numerical procedures have limited ability to reduce the total computational time necessary to simulate complex macromolecular systems.

For most of polymer systems, coarse-grained models are derived numerically. In general, the coarse-grained models build up from the atomic structure, lumping together groups of atoms into a larger effective particle. The simplest version among them is the united atom (UA) model, which groups atoms in the CH_2 monomer together into an effective united atom particle. This level of coarse-graining has been extensively employed in simulations of polymer liquids, and it has been proven to be quite successful in reproducing a large range of physical properties measured experimentally. The level of coarse-graining, however, is still very contained and the longest timescale that can be simulated, even by a set of computers working in parallel, is relatively short [32–36].

In specific cases, it is possible to derive *analytical* forms of the coarse-grained pair distribution functions from which input potentials for mesoscale simulations are derived by enforcing a closure approximation. These potentials do not suffer from the drawbacks of numerically derived ones, and they allow a transparent, often analytical, derivation of the thermodynamic properties for the coarse-grained system, e.g. the bulk compressibility. The derivation of analytical coarse-grained descriptions has been one of the main goals of our research, and in the following sections we present a couple of examples of analytical procedures to coarse-grain polymer liquids.

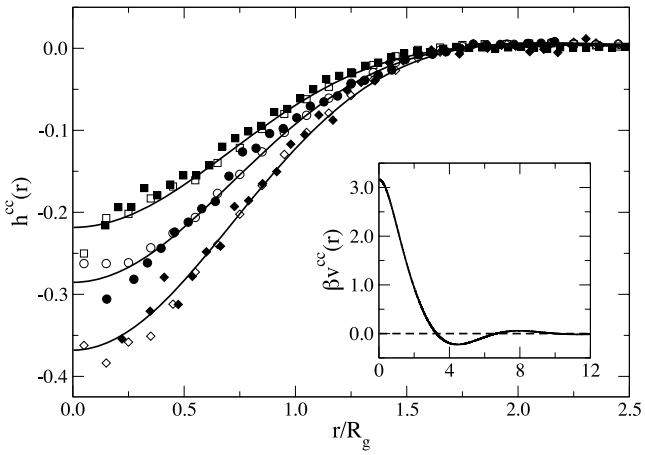

Figure 1. Plot of $h^{cc}(r)$ for PE melts with increasing N. Theory (full lines) is compared with UA (filled symbols) and mesoscale (open symbols) MD simulations for $N = 96$ (squares), 66 (circles), and 44 (diamonds). Inset shows $v^{cc}(r)$ for the $N = 44$ melt. Reprinted figure with permission from [26]. Copyright 2004 by the American Physical Society.

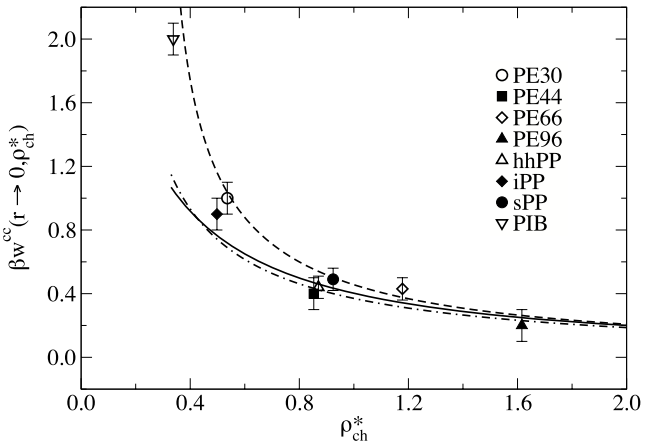

Figure 2. Potential of mean force at contact, $w^{cc}(0, \rho^*_{ch})$. Shown are the limits from equations (26) (solid line), (27) (dashed line), and (28) (dot–dashed line), as well as UA-MD data (symbols) with error bars. Reprinted with permission from [27]. Copyright 2006, American Institute of Physics.

2.4. Mapping homopolymers into interacting soft colloidal particles

One of the most popular coarse-grained description of polymer liquids models polymer coils as interpenetrable soft spheres, centered at the position of the polymer center of mass, and interacting through a realistic soft-core potential. This description affords an analytical form of the pair distribution function for the coarse-grained system. For this model, Dautenhahn and Hall [37] derived numerical solutions of the effective potentials for polymer melts and blends. More recently, Murat and Kremer [38] put forward a soft ellipsoid model for Gaussian polymer chains, which was later extended by Eurich and Maass [39]. For dilute solutions, Flory and Krigbaum [40] obtained a mean-field derivation of the potential between the centers of mass of a pair of polymers. Their mean-field approach predicts a potential at contact that increases with the degree of polymerization, in disagreement with computer simulations (see, for example, figures 1 and 2). Flory's model is inconsistent with simulations because, in his mean-field model, chains are not supposed to interpenetrate and the monomer–monomer repulsive interaction adds up to a stronger repulsion as the number of monomer increases. In reality, polymers are fractal objects of dimension $d = 2$, and a chain that occupies a region in three dimensions can fill its volume only partially. As a consequence, the monomer density ρ in the volume occupied by a chain, R_g^3, decreases with an increasing of degree of polymerization like $\rho \propto N/R_g^3 \propto N^{-1/2}$. Renormalization group calculations [41] and scaling theory [42], correctly predict a vanishing, but finite, potential at contact in the asymptotic $N \to \infty$ regime.

In a recent series of papers, Hansen and co-workers presented for dilute and semi-dilute solutions of interacting polymers, an effective state-dependent pair potential between the polymer centers of mass. The potential is numerically derived from the pair distribution function obtained from lattice Monte Carlo simulations, by applying an HNC approximation. Solutions are investigated in a range of densities and temperatures, and from good-to poor-solvent conditions. The potential at low density results from a sum of effective Gaussian repulsive pairwise interactions between two polymers. As the density increases, the potential develops a shallow negative tail for intermolecular distances larger than R_g [43]. At low polymer density, the dilute polymer solutions map into the well-known problem of a liquid of particles interacting through a repulsive Gaussian-core potential, which has been extensively investigated in the past by Stillinger, Weber and co-workers [44]. The Gaussian-core system shows in a specific low-temperature, low-density limit a re-entrant phase transition.

For liquids of homopolymer chains, we derived an analytical expression for the total pair correlation function (cfs) for interacting polymers coarse-grained at the center of mass level. The general expressions for the pair correlation functions involve com (c) and monomer (m) sites, $h^{cc}(r)$ and $h^{cm}(r)$. For a homopolymer fluid of molecular number density, ρ_{ch}, where each chain consists of N monomers, $h^{cc}(r)$ is obtained by solving four coupled Ornstein–Zernike (OZ) equations in reciprocal space involving real (monomer) and auxiliary (com) sites [45]. The respective matrix arrangement reads

$$\begin{aligned}\mathbf{C}(k) &= \mathbf{\Omega}^{-1}(k)\mathbf{H}(k)\mathbf{S}^{-1}(k)\\ &= \mathbf{\Omega}^{-1}(k) - \mathbf{S}^{-1}(k),\end{aligned} \tag{11}$$

where $\mathbf{C}(k)$ is the matrix of intermolecular direct cfs, $\mathbf{\Omega}(k)$ is the matrix of intramolecular cfs, $\mathbf{H}(k)$ is the matrix of intermolecular total pair cfs, and $\mathbf{S}(k) = \mathbf{\Omega}(k) + \mathbf{H}(k)$ is the matrix of partial cfs, also known as the static structure factor matrix.

All matrices in equation (11) have similar form, where monomer/monomer (mm) and com/com (cc) site contributions define diagonal elements, while cross contributions (cm/mc) define off-diagonal elements. For a macromolecular liquid, where each chain is sufficiently long that its intramolecular

monomer distribution obeys Gaussian statistics and chain end effects are negligible, it is useful to postulate that all monomer sites along a polymer chain are equivalent [24]. In this way, intramolecular and intermolecular cf matrices simplify to a single matrix element, thus facilitating the solution of the OZ equation. This approximation increases in accuracy with increasing degree of polymerization and is essential at rendering the original site-specific problem into an analytically tractable one. The assumption is better justified on the grounds that our approach focuses on coarse-grained functions, where monomer degrees of freedom are averaged in a mean-field manner.

Krakoviack *et al* [45] proposed a solution to equation (11) under the hypothesis that the com auxiliary site of one molecule does not interact directly with either the com or the monomers of another molecule (i.e. $c^{\mathrm{mm}}(k)$ is the only non-vanishing element in $\mathbf{C}(k)$). With this assumption, the solution is given by

$$h^{\mathrm{cc}}(k) = \left[\frac{\omega^{\mathrm{cm}}(k)}{\omega^{\mathrm{mm}}(k)}\right]^2 h^{\mathrm{mm}}(k), \tag{12}$$

where $h^{\mathrm{mm}}(k)$ is the total pair intermolecular monomer/monomer cf, $\omega^{\mathrm{cm}}(k)$ is the intrachain cf of monomers about the com, and $\omega^{\mathrm{mm}}(k)$ is the intramolecular monomer/monomer cf. Use has been made of the properties that $\omega^{\mathrm{cc}}(k) = 1$ (since the com bears no internal structure), $\omega^{\mathrm{cm}}(k) = \omega^{\mathrm{mc}}(k)$, and $S^{\mathrm{cm}}(k) = S^{\mathrm{mc}}(k)$. Moreover, $S^{\mathrm{mm}}(k) = \omega^{\mathrm{mm}}(k) + N\rho_{\mathrm{ch}}h^{\mathrm{mm}}(k)$, $S^{\mathrm{cm}}(k) = \omega^{\mathrm{cm}}(k) + N\rho_{\mathrm{ch}}h^{\mathrm{cm}}(k) = S^{\mathrm{mc}}(k)$, and $S^{\mathrm{cc}}(k) = 1 + \rho_{\mathrm{ch}}h^{\mathrm{cc}}(k)$. The definition of $S^{\mathrm{cc}}(k)$ formally corresponds to that of a simple liquid. Consistent with equation (12), the com/monomer total pair cf reduces to the simplified form,

$$h^{\mathrm{cm}}(k) = \left[\frac{\omega^{\mathrm{cm}}(k)}{\omega^{\mathrm{mm}}(k)}\right] h^{\mathrm{mm}}(k). \tag{13}$$

Both equations (12) and (13) are entirely general and hold for any macromolecular fluid.

In our coarse-graining approach, intramolecular correlations establish the bridging between mesoscopic and monomeric intermolecular correlations. For long molecular chains, the intramolecular monomer/monomer form factor follows Gaussian statistics, which is described well by the Debye formula [46],

$$\omega^{\mathrm{mm}}(k) = \frac{2N(\mathrm{e}^{-k^2R_{\mathrm{g}}^2} + k^2R_{\mathrm{g}}^2 - 1)}{k^4R_{\mathrm{g}}^4}, \tag{14}$$

R_{g} is the radius of gyration of the molecule. For mathematical convenience, however, it is customary to represent equation (14) using the corresponding Padé approximant [46],

$$\omega^{\mathrm{mm}}(k) \approx \frac{N}{1 + k^2R_{\mathrm{g}}^2/2}. \tag{15}$$

The com/monomer intramolecular form factor, $\omega^{\mathrm{cm}}(k)$, is defined as the Fourier transform of the distribution for a 'generic' monomer unit about the molecular com site. Specifically, the latter is derived by performing an average over all units and normalizing the distribution in real space of all 'specific' monomeric units j about the com. The probability function in real space reads [47]

$$P(\mathbf{r}_j) = \left(\frac{3}{2\pi\langle r_j^2\rangle}\right)^{3/2} \mathrm{e}^{-3r_j^2/(2\langle r_j^2\rangle)}, \tag{16}$$

where $\mathbf{r}_j$ represents the vector between segment j and the com. The mean square distance from segment j to the com is given by

$$\langle r_j^2\rangle = \frac{N\sigma^2}{3}\left[1 - \frac{3j(N-j)}{N^2}\right], \tag{17}$$

which takes into account the feature that end segments in a chain are on average located remotely from the com. The segment density distribution function for a generic monomer about the com can be accurately rendered by the well-known Gaussian form factor [47],

$$\omega^{\mathrm{cm}}(k) = N\mathrm{e}^{-k^2R_{\mathrm{g}}^2/6}. \tag{18}$$

When compared against simulation data, we observe that equation (18) approximates in good fashion all test systems. [27] However, the choice of equation (15) over (14) has the advantage of providing an analytically tractable equation at the expense of only a slight disagreement between theory and simulation data. In conclusion, to achieve an analytical solution of equations (12) and (13), we adopt as input equations (15) with (18). These equations together ensure analyticity and a reasonable agreement with UA-MD simulations.

At the monomer level, the total pair distribution function, $h^{\mathrm{mm}}(r)$, is modeled using Curro and Schweizer's polymer reference interaction site model (PRISM) [24, 25]. The polymer is described as a 'thread', in analogy with Edwards' field theoretic methods [49], i.e. a chain of vanishing thickness, infinite length, and constant monomer density. In PRISM, the OZ equation for the monomer total pair cf is solved by ignoring chain end effects and enforcing a hard-core Percus–Yevick-like closure, i.e. $c^{\mathrm{mm}}(k) = c^{\mathrm{mm}}(0) = c_0$ with $h^{\mathrm{mm}}(r \to 0) = -1$ and $c^{\mathrm{mm}}(r > 0) = 0$. The solution of the monomer-level OZ equation yields the simple form

$$h^{\mathrm{mm}}(r) = \frac{\xi_\rho'}{r}\left[\exp\left(-\frac{r}{\xi_\rho}\right) - \exp\left(-\frac{r}{\xi_{\mathrm{c}}}\right)\right], \tag{19}$$

where ξ_ρ is the length scale of density fluctuations defined as $\xi_\rho^{-1} = \xi_{\mathrm{c}}^{-1} + \xi_\rho'^{-1}$, and $\xi_\rho' = R_{\mathrm{g}}/(2\pi\rho_{\mathrm{ch}}^*)$ with $\rho_{\mathrm{ch}}^* \equiv \rho_{\mathrm{ch}}R_{\mathrm{g}}^3$ being the reduced molecular number density. Moreover, $\xi_{\mathrm{c}} = R_{\mathrm{g}}/\sqrt{2}$ is the length scale of the correlation hole [48].

In the thread model, $h^{\mathrm{mm}}(r)$ does not describe solvation shells observed on the local scale in macromolecular liquids, which result from hard-core excluded volume monomer interactions. On the other hand, the thread model captures correctly the correlation hole effect on the length scale of R_{g}, which is a feature characteristic of liquids of macromolecules [48]. Since $r \geqslant R_{\mathrm{g}}$ is the relevant length scale for the mesoscopic properties of interest here, the thread model works well for our coarse-graining purposes, and coupled with

the Padé approximant, it allows for an analytical solution of the OZ equation. We obtained intermolecular monomer–com, h^{cm}, and com–com, h^{cc}, total correlation functions, which are simply expressed in real space as the following analytical functions [26, 27, 50]

$$h^{\mathrm{cm}}(r, R_{\mathrm{g}}) = I^{\rho}(r, R_{\mathrm{g}}), \tag{20}$$

with

$$I^{\rho}(r, R) = -\frac{\xi'_{\rho}}{2r}(1 - \xi_{\mathrm{c}}^2/\xi_{\rho}^2)\mathrm{e}^{R^2/(6\xi_{\rho}^2)} \times \left[\mathrm{e}^{r/\xi_{\rho}}\mathrm{erfc}\left(\frac{R}{\sqrt{6}\xi_{\rho}} + \frac{\sqrt{3}r}{\sqrt{2}R}\right) - \mathrm{e}^{-r/\xi_{\rho}}\mathrm{erfc}\left(\frac{R}{\sqrt{6}\xi_{\rho}} - \frac{\sqrt{3}r}{\sqrt{2}R}\right)\right], \tag{21}$$

and

$$h^{\mathrm{cc}}(r, R_{\mathrm{g}}) = J^{\rho}(r, R_{\mathrm{g}}) \tag{22}$$

with

$$J^{\rho}(r, R) = \frac{3}{2}\sqrt{\frac{3}{\pi}}\frac{\xi'_{\rho}}{R}\left(\frac{\xi_{\mathrm{c}}}{R}\right)^2\left(1 - \frac{\xi_{\mathrm{c}}^2}{\xi_{\rho}^2}\right)\mathrm{e}^{-3r^2/(4R^2)} - \frac{\xi'_{\rho}}{2r}(1 - \xi_{\mathrm{c}}^2/\xi_{\rho}^2)\mathrm{e}^{R^2/(3\xi_{\rho}^2)}\left[\mathrm{e}^{r/\xi_{\rho}}\mathrm{erfc}\left(\frac{R}{\sqrt{3}\xi_{\rho}} + \frac{\sqrt{3}r}{2R}\right) - \mathrm{e}^{-r/\xi_{\rho}}\mathrm{erfc}\left(\frac{R}{\sqrt{3}\xi_{\rho}} - \frac{\sqrt{3}r}{2R}\right)\right]. \tag{23}$$

Those reduce, in the limit of long polymer chains, to the following equations

$$h^{\mathrm{cm}}(\tilde{r}, \tilde{\xi}_{\rho}) \approx -\frac{3}{2}\sqrt{\frac{6}{\pi}}\tilde{\xi}_{\rho}\left(1 + \sqrt{2}\tilde{\xi}_{\rho}\right) \times \left[1 + \mathcal{O}\left(\tilde{\xi}_{\rho}^2, \tilde{r}^2\right)\right]\mathrm{e}^{-3\tilde{r}^2/2}, \tag{24}$$

and

$$h^{\mathrm{cc}}(\tilde{r}, \tilde{\xi}_{\rho}) \approx -\frac{39}{16}\sqrt{\frac{3}{\pi}}\tilde{\xi}_{\rho}\left(1 + \sqrt{2}\tilde{\xi}_{\rho}\right) \times \left[1 - \frac{9\tilde{r}^2}{26} + \mathcal{O}\left(\tilde{\xi}_{\rho}^2, \tilde{r}^4\right)\right]\mathrm{e}^{-3\tilde{r}^2/4}. \tag{25}$$

Here $\tilde{r} = r/R_{\mathrm{g}}$ is the normalized intermolecular distance and $\tilde{\xi}_{\rho} = \xi_{\rho}/R_{\mathrm{g}}$ is the normalized length scale of density fluctuations, with ξ_{ρ} defined as $\xi_{\rho}^{-1} = \xi_{\mathrm{c}}^{-1} + \xi_{\rho}'^{-1}$, where $\xi'_{\rho} = 3/(\pi\rho\sigma^2)$. Moreover, $\xi_{\mathrm{c}} = R_{\mathrm{g}}/\sqrt{2}$ is the length scale of the correlation hole. The normalized total correlation functions, $h^{\mathrm{cc}}(\tilde{r}, \tilde{\xi}_{\rho})/\tilde{\xi}_{\rho}$ and $h^{\mathrm{cm}}(\tilde{r}, \tilde{\xi}_{\rho})/\tilde{\xi}_{\rho}$, become universal functions of the reduced distance $\tilde{r}$ when higher-order corrections in $\tilde{\xi}_{\rho}$ are negligible, i.e. for large N.

Equations (20)–(25) formally relate the structure of the liquid on a mesoscopic level to microscopic molecular parameters, such as statistical segment length, σ, and radius of gyration, R_{g}, as well as to the thermodynamic parameters of temperature, as $\sigma(T)$, and density, ρ. In principle, equation (22) is apt to describe the mesoscopic structure of polymer solutions from the melt to the dilute regime, given that it satisfies the condition that $h^{\mathrm{cc}}(r) \geqslant -1$ in the whole range of melt-like densities down to $\rho^*_{\mathrm{ch}} = \rho_{\mathrm{ch}}R_{\mathrm{g}}^3 \gtrsim 0.03$, where $\rho_{\mathrm{ch}} = \rho/N$. Restrictions on the range of ρ^*_{ch}, on the other hand, do not exist for equation (20).

To test the quality of our theoretical predictions we directly compared equations (22) and (25) against the total correlation functions calculated from united atom molecular dynamics simulations of melts of polyethylene chains. Test systems were melts of polymers with increasing degree of polymerization, $N = 44$ ($T = 400$ K, $\rho = 0.0324$ sites Å^{-3}), $N = 66$ ($T = 448$ K, $\rho = 0.0329$ sites Å^{-3}) and 96 ($T = 453$ K, $\rho = 0.0328$ sites Å^{-3}). Simulation trajectories for those systems were kindly provided by Grest and co-workers [51]. When compared against simulation data, figure (1) shows that both the exact, equation (22), and the approximate, equation (25), analytical expressions for the total correlation functions reproduce well UA-MD simulations. This is a remarkable result because the theoretical calculations do not contain any adjustable parameter.

The same quality of agreement was also observed for polyethylene in reciprocal space [26, 27], as well as for melts of polymers with different monomer architecture in both real and reciprocal spaces, including polyisobutylene (PIB) and polypropylenes in their head-to-head (hhPP), isotactic (iPP), and syndiotactic (sPP) forms [33, 50, 51]. We also found that exact, equation (20), and approximate, equation (24), analytical expressions for the monomer–com total correlation functions reproduce equally well UA-MD simulations, in both real and reciprocal space [27]. Furthermore, the analytical total correlation functions correctly predict thermodynamic properties of the liquid, such as the isothermal compressibility from the Fourier transform of the $k \to 0$ limit of the mesoscopic static structure factor, where $S^{\mathrm{cc}}(0) = 1 + \rho_{\mathrm{ch}}h^{\mathrm{cc}}(0) = (\xi_{\rho}/\xi_{\mathrm{c}})^2 = S^{\mathrm{mm}}(0)/N$ while $S^{\mathrm{cm}}(0) = N + N\rho_{\mathrm{ch}}h^{\mathrm{cm}}(0) = N(\xi_{\rho}/\xi_{\mathrm{c}})^2 = S^{\mathrm{mm}}(0)$, as well as the equation of state via the compressibility route [52].

Finally, we calculated the potential of mean force, which represents the effective interaction between a pair of coarse-grained units *in the mean field* of the surrounding particles, and it is defined as $\beta w^{\mathrm{cc}}(r) = -\ln[1+h^{\mathrm{cc}}(r)]$, with $\beta = (k_{\mathrm{B}}T)^{-1}$. The resulting potential has a Gaussian-like repulsive shape with a slightly attractive contribution and a range of order R_{g}. The potential at contact is

$$\beta w^{\mathrm{cc}}(0) = -\ln\left[1 - \frac{3}{8}\sqrt{\frac{3}{\pi}}\left(\frac{1 + \sqrt{2}\tilde{\xi}_{\rho}}{\tilde{\xi}_{\rho}}\right) \times \left\{1 + \frac{4}{3}\left(1 - \frac{1}{2\tilde{\xi}_{\rho}^2}\right)\left(1 - \frac{\sqrt{\pi}\mathrm{e}^{1/(3\tilde{\xi}_{\rho}^2)}}{\sqrt{3}\tilde{\xi}_{\rho}} \times \mathrm{erfc}\left[\frac{1}{\sqrt{3}\tilde{\xi}_{\rho}}\right]\right)\right\}\right], \tag{26}$$

which, in the large-N limit, reads

$$\beta w^{\mathrm{cc}}(0) \approx -\ln\left[1 - \frac{39}{16}\sqrt{\frac{3}{\pi}}\tilde{\xi}_{\rho}\left(1 + \sqrt{2}\tilde{\xi}_{\rho}\right)\right] \tag{27}$$

$$\approx \frac{39}{16}\sqrt{\frac{3}{\pi}}\tilde{\xi}_{\rho}, \tag{28}$$

which presents the correct trend of increasing chain interpenetration with increasing density, degree of polymerization, and local stiffness. Figure 2 shows a comparison of $w^{cc}(0)$ as predicted by theory and observed in simulations for all polymer we investigated [26, 27, 50]. The response as $r \to 0$ is evaluated from simulation data with an algorithm that minimizes the influence of outliers, a necessity due to poor statistics in this regime. Error bars depicted in figure 2 are based on results from the fitting routine. Approximate and exact forms of $w^{cc}(0)$ become practically indistinguishable when $N \gtrsim 30$ and at melt-like densities, for linear and slightly branched polymer chains. The observed trend of the potential at contact with degree of polymerization is consistent with the predictions of renormalization group calculations [41] and scaling theory [42].

2.5. *Effective mesoscale potentials for homopolymer liquids*

The effective interaction potential between two coarse-grained units, $v^{cc}(r)$, is obtained from equations (20) and (22) by enforcing the HNC closure, which is accurate for systems characterized by long-range, soft-core potentials. Figure (1) shows, as an example, the effective potential for a liquid of polyethylene molecules with $N = 44$ monomers. The potential, so derived, is given by a Gaussian repulsive interaction, which includes a shallow attractive tail. We found that the presence of the attractive contribution in the potential is relevant for the thermodynamic properties of the liquid, because it is responsible for the stabilization of the liquid phase [52]. Furthermore, the potential at contact remains finite, which is consistent with the fact that a pair of center of mass sites can overlap without violating excluded volume constraints. Finally, the potential is system specific, because it is able to distinguish between chemically different polymers. In this way, the coarse-grained model retains the chemical identity of the parent polymer [50].

Using the potential so derived, we implemented classical molecular dynamics simulations of the coarse-grained system, which is a liquid of interacting soft colloidal particles. Simulations were performed within the microcanonical ensemble (N, V, E fixed) and the results for the total correlation functions are reported in figure 1. The agreement between united atom and mesoscale simulations is excellent and consistent with the theoretical predictions of equations (22) and (25).

Structure and dynamics[1] as predicted by the simulations of the system coarse-grained at the two different levels are completely consistent, with the structure sampled as the center of mass distribution function and when dynamics is properly rescaled and analyzed for length scales larger than the radius of gyration. However, while UA-MD simulations require ≈24 h for a system with 1600 particles performed in parallel on a 64-node cluster, for the equivalent trajectory our mesoscale simulations requires only ≈4 h for a system consisting of ≈6000 particles on a single-CPU workstation, which compares extraordinarily well. In conclusion, large-scale properties of homopolymer melts appear to be well represented by liquids of soft interacting colloidal particles, while simulations of the coarse-grained systems afford a clear advantage in computational time.

[1] The systems presented here are not entangled.

2.6. *Analytical coarse-graining of homopolymer mixtures*

When two or more types of polymers are mixed together, new materials emerge with specific physical and chemical properties. It is often possible to custom-tailor materials by simply blending polymer components that possess desirable features. For instance, upon mixing brittle polystyrene with non-crystalline polyethylene oxide, a new substance is produced that is tough yet possesses a highly elastic modulus. Although polymer blends have been very much a part of everyday life for a long time, they continue to be a source of great scientific interest for their many scientific and technological properties [24, 25, 32, 33, 36, 53–60].

Computer simulations have yielded a great deal of information on the correlation between local (intramolecular and intermolecular) structure and global fluid properties. One of the challenges in simulating polymer blends is the large range of length and timescales that need to be investigated, spanning from the local chemical structure to the length scale of concentration fluctuations, which diverges as they approach their spinodal decomposition.

Coarse-graining of polymer blends in conjunction with multiscale modeling, is a possible solution to this issue. In our coarse-graining procedure, polymer blends are mapped into binary mixtures of interacting soft, colloidal particles centered at the polymer center of mass. The binary blend consists of a mixture of A and B homopolymers, having N_A and N_B monomer sites with segment lengths σ_A and σ_B, respectively, and $\gamma = \sigma_B/\sigma_A$. For simplicity, these monomer sites are taken to span equivalent volumes, so that the polymer volume fraction is given by $\phi = n_A N_A/(n_A N_A + n_B N_B)$, where n_α is the number of molecules of type α in the mixture with $\alpha \in \{A, B\}$. While $\rho_m = (n_A N_A + n_B N_B)/V$ quantifies the total number of monomer sites contained in a region of space spanned by V, the site and chain number densities for molecules of type α are given by $\rho_{m,\alpha} = n_A N_A/V = \phi\rho_m$ and $\rho_{c,\alpha} = n_A/V$, respectively.

Total correlation functions are calculated from the Ornstein–Zernike equation, which includes monomers and center of mass sites, and has a matrix form with diagonal blocks containing self-contributions, whereas cross contributions occupy off-diagonal positions. Direct interactions involving auxiliary sites are set to zero, in an extension of the procedure described in the previous section.

Self-intermolecular and cross intermolecular total correlation functions are given as [61]

$$\begin{aligned} h^{cc}_{AA}(r) &= \frac{1-\phi}{\phi} I^{\phi}_{AA}(r) + \gamma^2 I^{\rho}_{AA}(r), \\ h^{cc}_{BB}(r) &= \frac{\phi}{1-\phi} I^{\phi}_{BB}(r) + \gamma^{-2} I^{\rho}_{BB}(r), \\ h^{cc}_{AB}(r) &= -I^{\phi}_{AB}(r) + I^{\rho}_{AB}(r), \end{aligned} \tag{29}$$

where $I^{\phi}_{\alpha\beta}(r)$ and $I^{\rho}_{\alpha\beta}(r)$ identify the concentration and density fluctuation contributions, respectively. We introduce here a compact notation with the function $I^{\lambda}_{\alpha\beta}(r)$ defined as

$$I^{\lambda}_{\alpha\beta}(r) = \frac{3}{4}\sqrt{\frac{3}{\pi}}\frac{\xi'_{\rho}}{R_{g\alpha\beta}}\left(1-\frac{\xi^2_{c\alpha}\xi^2_{c\beta}}{\xi^2_{c\alpha\beta}\xi^2_{\lambda}}\right) \times e^{-3r^2/(4R^2_{g\alpha\beta})} - \frac{1}{2}\frac{\xi'_{\rho}}{r}\left(1-\frac{\xi^2_{c\alpha}}{\xi^2_{\lambda}}\right) \times \left(1-\frac{\xi^2_{c\beta}}{\xi^2_{\lambda}}\right) e^{R^2_{g\alpha\beta}/(3\xi^2_{\lambda})}\left[e^{r/\xi_{\lambda}}\,\mathrm{erfc}\left(\frac{R_{g\alpha\beta}}{\xi_{\lambda}\sqrt{3}}+\frac{r\sqrt{3}}{2R_{g\alpha\beta}}\right) - e^{-r/\xi_{\lambda}}\,\mathrm{erfc}\left(\frac{R_{g\alpha\beta}}{\xi_{\lambda}\sqrt{3}}-\frac{r\sqrt{3}}{2R_{g\alpha\beta}}\right)\right] \quad (30)$$

and where $\xi_{\lambda} \in \{\xi_{\phi}, \xi_{\rho}\}$ and $\xi'_{\rho} = 3/(\pi\rho\sigma^2_{AB})$, while the radii of gyration entering the blend equation are defined as $R^2_{g\alpha\beta} = (R^2_{g\alpha} + R^2_{g\beta})/2 = 2\xi^2_{c\alpha\beta}$. The length scale governing concentration fluctuations is

$$\xi_{\phi} = \frac{\sigma_{AB}}{\sqrt{24\phi(1-\phi)(\chi_s-\chi)}}, \quad (31)$$

which diverges at the spinodal temperature, since $\chi \approx \chi_s$. The parameter χ is the analog of the Flory–Huggins interaction parameter given by $\chi = \epsilon_{AB} - (\epsilon_{AA} + \epsilon_{BB})/2 \propto T^{-1}$, while $\chi_s = [2N_A\phi]^{-1} + [2N_B(1-\phi)]^{-1}$ defines the spinodal temperature.

Also, $\xi_{c\alpha} = R_{g\alpha}/2^{1/2}$ is the length scale of the correlation hole while $\xi^{-1}_{\rho\alpha\beta} = \pi\rho\sigma^2_{\alpha\beta}/3 + \xi^{-1}_{c\alpha\beta}$ is the density correlation length scale with $\sigma^2_{\alpha\beta} = \phi_{\beta}\sigma^2_{\alpha} + \phi_{\alpha}\sigma^2_{\beta}$. This latter definition reintroduces finite size effects, local semiflexibility, and branching that pertain to each component through a melt-like description. The effective segment length scale is determined from the radius of gyration of each component, through the relation $\sigma_{\alpha} = (6/N_{\alpha})^{1/2}R_g$. Equation (29) formally connects center of mass distribution functions to monomer–monomer intramolecular and intermolecular distribution functions. In this manner, one calculates mesoscale properties from information on the local polymer scale. As previously mentioned, this feature is important because it correlates mesoscale properties to microscopic parameters. Because the formalism of equation (29) is analytical, it affords all the advantages previously discussed of gain in computational time, transparent derivation of thermodynamic properties, and transferability of the representation. Analytical equations were derived also for the monomer–com total distribution functions [61].

Next, we compare our analytical expressions against data from UA-MD simulations of polymer blends [32, 33]. Figure 3 shows that for each blend considered, the theory agrees with simulation data fairly well. The center of mass total correlation function provides an estimate of the number of molecules interpenetrating at some relative distance r. In all the plots we observe that chains of the stiffest component (B), which have extended configurations, tend to pack at short distances $r < R_{gB}$ more efficiently than flexible ones. Flexible molecules, which have coiled configurations, show a high (low) number of intramolecular (intermolecular) contacts and pack most

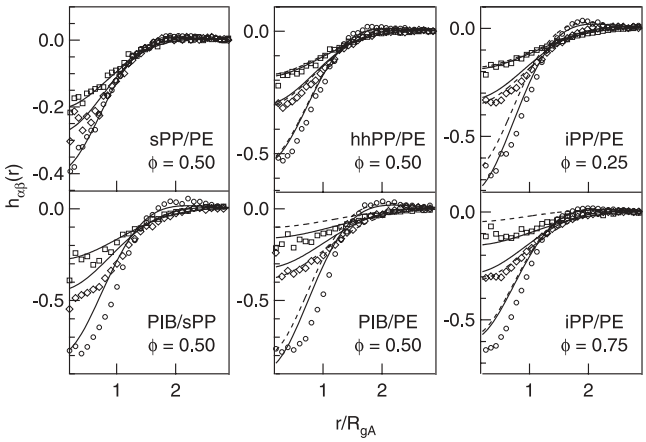

Figure 3. Plots of $h_{\alpha\beta}(r)$ against r/R_{gA} for blends. Theoretical predictions in athermal (full lines) and thermal (dashed lines) conditions are compared with UA-MD simulations of blends: AA—(circles), AB—(diamonds), and BB—terms (squares). Reprinted with permission from [61]. Copyright 2005, American Institute of Physics.

efficiently at distances on the order of the overall polymer size, $r \approx 1.5R_{gA}$. The extent of intermolecular chain packing upon blending also depends on the polymer flexibility. The theory predicts that the stiff (flexible) component packs better (worse), and the number of self-contacts increases (decreases) when mixed with a more flexible (stiffer) polymer, in agreement with simulations.

In general, the agreement between theory and simulations is good with the exception of the PIB/hhPP and PIB/iPP blends, for which agreement is only qualitative. For these systems, the theory overestimates the number of intermolecular contacts. However, it is well known that PIB blends are usually immiscible blends at these temperatures and for these chain lengths [33, 62]. PIB presents a very efficient intramolecular and intermolecular packing, which leads to a thermal expansion coefficient and an isothermal compressibility smaller than in other polyolefin blends [62]. This behavior is due to strong attractive interactions between the methyl ($-CH_3$) groups, which in PIB molecules are in very large number (about 50% of the total number of united atoms) [60]. However, even for PIB blends, the theory shows very good agreement with simulation data for $r \approx R_g$.

Finally, figure 4 shows that the theory is able to predict correct qualitative behavior also for blends that follow a LCST phase diagram. At high temperature the blend de-mixes and displays a distribution function for the AB component that is consistently lower than the AA and the BB contributions. At low temperature, instead, the mixing of the A and B species is enhanced with the AB function always higher than its AA and BB counterparts.

2.7. Mapping homopolymer blends into mixtures of soft interacting colloidal particles

We now show how our mesoscale description of polymer blends effectively maps the system onto a two-component mixture of colloidal particles by making a formal connection

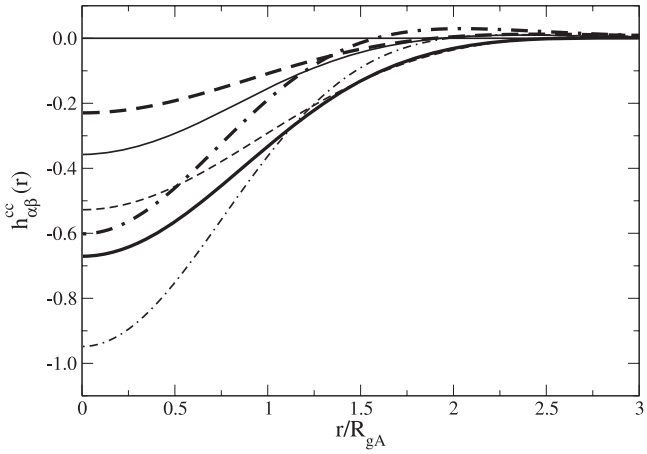

Figure 4. Plots of $h_{\alpha\beta}(r)$ against r/R_{gA} for a model blend described by $\chi = 0.011\,25 - 4.75/T$ ($N_A = 96$, $\rho_m = 0.034$ Å^{-3}, $\sigma_A = 2.44$ Å, $\phi = 0.50$, and $\chi_s = 0.021$). Shown are AA—(dot–dashed lines), AB—(full lines), and BB—terms (dashed lines) at two temperatures: $T = 150$ K (normal-weight lines) and $T = 10\,000$ K (heavy-weight lines). Reprinted with permission from [61]. Copyright 2005, American Institute of Physics.

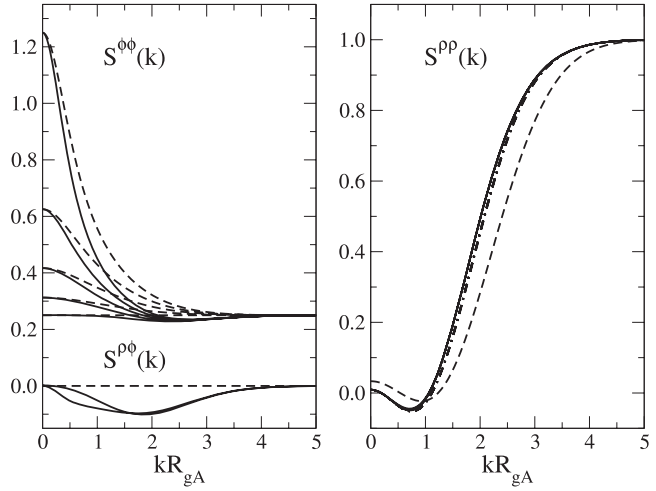

Figure 5. Plot of colloid static structure factors against kR_{gA} for $\gamma = 1.5$ (full lines) and $\phi = 0.5$. Also shown is the athermal symmetrical case (dashed lines). Left panel: upper portion, $S^{\phi\phi}(k)$ with $\chi/\chi_s \in \{0.0, 0.2, 0.4, 0.6, 0.8\}$ from bottom to top; lower portion, $S^{\rho\phi}(k)$ with $\chi/\chi_s = 0.0$ (top line) and $\chi/\chi_s = 0.8$ (bottom line). Right panel: $S^{\rho\rho}(k)$ and $S^{\rho\rho}(k) - \delta^2 S^{\phi\phi}(k)$ (dot–dashed lines, $\gamma = 1.5$; for $\gamma = 1.0$, $\delta = 0$) for the same values of χ/χ_s used in the left panel (curves are indistinguishable in the plot). Reprinted with permission from [61]. Copyright 2005, American Institute of Physics.

with well-known theories of liquid alloys [63, 64]. The mixture contains colloidal particles A and B with volume fraction $\phi = n_A/(n_A + n_B)$, total density $\rho_{ch} = \rho/N$, and particle size R_{gA} and R_{gB}. When species A is chosen to be our reference system, the size mismatch parameter is $\gamma = R_{gB}/R_{gA}$, and the reduced chain density is $\rho^*_{ch} = \rho_{ch} R^3_{gA}$. This renormalized description can be formally obtained from equations (29) by setting the effective number of statistical segments in the two components to be equal, $N_A = N_B = N$, while the chain asymmetry is completely accounted for by the different statistical segment lengths $\sigma'_A = R_{gA}\sqrt{6/N}$ and $\sigma'_B = R_{gB}\sqrt{6/N}$. Each effective segment includes the effect of branching and chain semiflexibility, and must be equal or larger than its polymer persistence length, a condition fulfilled by long semiflexible chains.

To make a connection with the theory of colloidal particle mixtures (liquid alloys), as developed by Bhatia and Thornton, [63] we calculated the linear combinations of the static structure factors for the mixture, which are defined as

$$\begin{aligned} S_{AA}(k) &= \phi + \phi^2 \rho_{ch} h_{AA}(k), \\ S_{BB}(k) &= 1 - \phi + (1-\phi)^2 \rho_{ch} h_{BB}(k), \\ S_{AB}(k) &= \phi(1-\phi)\rho_{ch} h_{AB}(k), \end{aligned} \tag{32}$$

and describe fluctuations in number density and concentration. The density fluctuation contribution (S^{NN} in the conventional notation for 'metal alloys') is given by

$$S^{\rho\rho}(k) = S_{AA}(k) + S_{BB}(k) + 2S_{AB}(k), \tag{33}$$

while the concentration fluctuation contribution (S^{CC}) is

$$\begin{aligned} S^{\phi\phi}(k) &= (1-\phi)^2 S_{AA}(k) + \phi^2 S_{BB}(k) \\ &\quad - 2\phi(1-\phi) S_{AB}(k), \end{aligned} \tag{34}$$

and their coupling (S^{CN}) is

$$\begin{aligned} S^{\rho\phi}(k) &= (1-\phi) S_{AA}(k) - \phi S_{BB}(k) \\ &\quad + (1-2\phi) S_{AB}(k). \end{aligned} \tag{35}$$

Figure 5 presents model calculations of equations (33)–(35), and illustrates how these equations follow closely the behavior in reciprocal space observed for simple colloidal mixtures. For example, $S^{\rho\rho}(k)$ has a k-dependence similar to the static structure factor for a single-component liquid. However, because our colloids are soft and can interpenetrate, there is no formation of solvation shells in the mixture, and $S^{\rho\rho}(k)$ becomes a monotonically increasing function of k. $S^{\phi\phi}(k)$ and $S^{\rho\phi}(k)$ oscillate about the values $\phi(1-\phi)$ and zero, respectively, as observed in colloidal mixtures with oscillations becoming less pronounced in $S^{\phi\phi}(k)$. A more intuitive picture of the density–concentration fluctuation coupling term can be achieved by rewriting it as [63]

$$\begin{aligned} S^{\phi\rho}(k) &= \phi(1-\phi)\rho_{ch} \int [P_A(r) - P_B(r)] \\ &\quad \times \frac{\sin(kr)}{kr} 4\pi r^2 \, \mathrm{d}r \end{aligned} \tag{36}$$

with $P_\alpha(r) = (1-\phi) g_{B\alpha}(r) + \phi g_{A\alpha}(r)$ the probability of encountering clustering of particles of species A or B around the colloid $\alpha \in \{A, B\}$. In this way, the function $S^{\phi\rho}(k)$ represents a measure of the difference in local clustering between species A and B. Maxima and minima in the function point at length scales characterized by large asymmetry in the liquid structure due to the mismatch in particle size. If the two species are identical, the mixture is uniform and $S^{\phi\rho}(k) = 0$ for any k.

In the $k \to 0$ limit, the density fluctuation contribution and its coupling with concentration fluctuations reduce to the simplified forms

$$S^{\rho\rho}(0) = \frac{\xi_\rho^2}{\xi_{cA}^2}\frac{\phi\gamma^2 + 1 - \phi}{\gamma^2}, \tag{37}$$

$$S^{\rho\phi}(0) = \phi(1-\phi)\frac{\gamma^2 - 1}{\gamma^2}\frac{\xi_\rho^2}{\xi_{cA}^2}, \tag{38}$$

while the concentration fluctuation contribution is

$$S^{\phi\phi}(0) = \frac{\phi(1-\phi)}{1 - \chi/\chi_s} + \frac{\phi^2(1-\phi)^2(\gamma^2-1)^2}{(\phi\gamma^2 + 1 - \phi)\gamma^2}\frac{\xi_\rho^2}{\xi_{cA}^2}. \tag{39}$$

For a blend of symmetric polymers, where $R_{gA} = R_{gB}$ and $\gamma = 1$, our equations become completely consistent with the theory for a mixture of symmetric colloidal particles [4, 63]. Equation (37) simplifies to $S^{\rho\rho}(0) = (\xi_\rho/\xi_{cA})^2$ the melt compressibility, $S^{\rho\phi}(0) = 0$, and the concentration fluctuation contribution becomes

$$S^{\phi\phi}(0) = \frac{\phi(1-\phi)}{1 - 2\phi(1-\phi)\Delta E}. \tag{40}$$

In this derivation, we made use of Flory's spinodal parameter, χ_s, and the renormalized χ parameter for the coarse-grained polymer mixture $\Delta E = N\chi = N\epsilon_{AB} - (N\epsilon_{AA} + N\epsilon_{BB})/2$. For long polymer chains or high density, equations (37), (38) vanish because $\xi_\rho/\xi_c \to 0$, while the concentration fluctuation contribution $S^{\phi\phi}(0) = \phi(1-\phi)/(1 - \chi/\chi_s)$.

In general, asymmetry between the two colloidal species is quantified by the dilation factor [64]

$$\delta = \frac{v_A - v_B}{\phi v_A + (1-\phi)v_B} = \frac{S^{\rho\phi}(0)}{S^{\phi\phi}(0)} = \frac{(\phi\gamma^2 + 1 - \phi)(\gamma^2 - 1)}{\phi(1-\phi)(\gamma^2-1)^2 + \gamma^2\xi_\phi^2/\xi_\rho^2}. \tag{41}$$

If the partial molar volumes per particle $v_\alpha = (\partial V/\partial n_\alpha)_{n_{\beta\neq\alpha}, P, T}$ of the two species are identical, $\delta = 0$ and $\gamma = 1$, there is no correlation between the fluctuations in particle number and concentration and $S^{\rho\phi}(k) = 0$. At the spinodal, $S^{\phi\phi}$ diverges and $\delta \to 0$.

The isothermal compressibility for a colloidal mixture is defined [64] as

$$\rho_{ch} k_B T \kappa_T = S^{\rho\rho}(0) - \frac{S^{\rho\phi}(0)^2}{S^{\phi\phi}(0)} = S^{\rho\rho}(0) - \delta^2 S^{\phi\phi}(0). \tag{42}$$

Here,

$$\rho_{ch} k_B T \kappa_T = \frac{\xi_\rho^2}{\xi_{cA}^2}\frac{\phi\gamma^2 + 1 - \phi}{\gamma^2} \times \left[1 - \frac{(\gamma^2-1)^2\phi(1-\phi)}{\phi(1-\phi)(\gamma^2-1)^2/\gamma^2 + \xi_\phi^2/\xi_\rho^2}\right], \tag{43}$$

recovers the melt compressibility when the system is composed of colloidal particles of identical size, $\gamma = 1$. The compressibility is slightly temperature dependent through the correction contribution due to $S^{\rho\phi}(0)^2/S^{\phi\phi}(0)$. The latter, however, is small for large polymer chains since it scales with degree of polymerization as N^{-1} in the athermal regime, and vanishes approaching the spinodal curve where the concentration fluctuation correlation length diverges. This is true at any length scale and the k-dependent blend 'compressibility' can be approximated by its first contribution $S^{\rho\rho}(k)$ in the entire range of k and for blends of polymer chains with symmetric or asymmetric size, in agreement with colloidal particle mixtures.

In conclusion, our coarse-graining theory displays a good predictive power, while it reproduces known predictions of established theories for colloidal mixtures, and good agreement with united atom computer simulations of homopolymer mixtures.

From the pair distribution functions we derived the respective effective potential for each pair of like and unlike molecules, $v_{\alpha\beta}^{cc}(r)$ with $\alpha\beta \in \{A, B\}$, by applying the HNC approximation as outlined in our approach for polymer melts. The $v_{\alpha,\beta}^{cc}(r)$ so obtained were used as an input to simulations of coarse-grained polymer mixtures, where each polymer was represented as an interacting soft colloidal particle. Once more, the results of mesoscale simulations of polymer mixtures were found to reproduce center of mass total correlation functions, as calculated from united atom computer simulations, within numerical error [65].

2.8. Analytical coarse-graining models for diblock copolymer liquids

Diblock copolymers are systems of great interest for their technological applications [66, 67]. Because the two blocks are chemically different, they experience a repulsive interaction that would encourage phase separation at low temperatures where entropy cannot balance enthalpic effects. However, the chemical bond existent between the two blocks prevents a complete separation of the two phases. As a consequence, at low temperatures block copolymer liquids undergo a microphase transition from disordered systems to ordered microstructures of nanoscopic size, namely the microphase separation transition (MST). The length scale characterizing the size of the microphase is of the order of the block radius of gyration.

Developing the technology to produce micro-ordered structures of well-controlled size and shape requires an understanding of the processes that drive the formation of micro-ordered phases under different thermodynamic conditions of temperature T and density ρ, as well as different chain composition f, monomer structure σ, and degree of polymerization N. Coarse-graining models of block copolymer molecules in conjunction with multiscale approaches, are useful for simulating their properties on the large range of time and space scales of interest.

We proposed the coarse-graining of diblock copolymer liquids as liquids of interacting soft colloidal dumb-bells. Each dumb-bell represents one macromolecule composed by two effective soft colloidal particles, having the dimensions of the block radii of gyration, and centered on the coordinates of the center of mass of each block. Total distribution functions

for three different length scales are formally related in our analytical approach, which corresponds to coarse-graining the molecule at the monomer (the statistical segment length, σ), block (the radius of gyration of block A, R_{gA}), and polymer (the polymer radius of gyration, R_g) scales. In this way, our theory represents a mesoscopic model of polymeric liquid structures where total correlation functions are resolved at three different *intramolecular* length scales.

In the recent years, there has been a growing interest in developing coarse-graining models for block copolymers chains [68–70]. Building blocks of supermolecular structures, such as cellular membranes, have been modeled as self-assembling block copolymers chains [71]. A recent paper by Hansen and co-workers proposes a model of coarse-graining for a symmetric diblock copolymer similar to ours, as the chain is modeled as two soft blobs, tethered by an entropic spring [72]. The blobs have equal size, and the coarse-grained total distribution functions are calculated numerically from a Monte Carlo simulation of diblock copolymers described at the monomer level. Monomers occupy the sites of a simple cubic lattice, with bond along the x- , y- , or z-directions. The two blocks individually are modeled as if they where in theta solvent, while the interaction between them is self-avoiding. The numerical inversion procedure to derive the coarse-grained potential is performed in the athermal regime. As the authors point out in the paper, their model is 'highly simplified', which proves the difficulty in treating intramolecular coarse-graining. The model, coupled with a reference interaction site model (RISM) and a random-phase approximation closure, predicts the mean-field clustering of diblock copolymers in a selective solvent [73].

Our model differs from the one presented in [72] in several ways. In our case, the size of the two 'blobs' varies depending on the chain composition, f, degree of polymerization, N, and segment length, σ. Moreover, repulsive interactions between segments of different chemical nature are quantified by the interaction parameter, χ_{eff}. Concentration fluctuation stabilization enters through the polymer reference interaction site model (PRISM) theory for the monomer-level description [24, 74, 75], and deviations from mean-field theory [76] are predicted by our coarse-grained approach as well. The two blocks follow Gaussian intramolecular statistics, which is a good approximation for copolymer melts, when each block has a degree of polymerization $N_\alpha > 30$, with $\alpha \in A, B$, and for the region in the phase diagram from the high temperature to the weak segregation regime ($\chi_{\text{eff}}N \ll 10.5$ for symmetric composition $f = 0.5$), where the system is isotropic. Numerical mean-field theory studies suggest coil stretching is not significant even below the order–disorder transition until a strong segregation regime is entered, where $\chi_{\text{eff}}N \geqslant 100$ [77, 78].

Segments of different chemical nature are assumed to have equivalent statistical lengths, $\sigma_A = \sigma_B = \sigma$, while the specific chemical nature of the block enters through the block radius of gyration. Segments of like species interact through the potentials $v_{AA} \approx v_{BB}$, while unlike species repel each other through v_{AB}. At high temperatures, entropic effects dominate over enthalpic contributions, and block copolymer liquids resemble closely liquids of homopolymer molecules. As the temperature decreases, the effective repulsive potential $\chi_{\text{eff}} = v_{AA} + v_{BB} - 2v_{AB}$ increases as $N\chi_{\text{eff}} \propto T^{-1}$, leading to the phase separation transition. This phase transition is characterized by a dramatic increase of the collective concentration fluctuation static structure factor, $S^\phi(k^*)$, at a specific length scale, k^* [76]. At the temperature of the phase transition, only certain fluctuations become anomalously large and the liquid segregates on a molecular length scale on the order of the overall size of the molecule, $k^* \sim R_g^{-1}$. This remarkable property of copolymer liquids is due to the fact that, because of the connectivity between different blocks, even complete segregation cannot lead to macroscopic phase separation, as occurs in mixtures of two chemically different homopolymer melts [79, 80]. Because even at high temperatures, $S^\phi(k)$ presents a peak due to the finite molecular size of the block copolymer chain, the peak position is largely independent of temperature. Moreover, finite size effects suppress concentration fluctuations leading to a first-order phase transition. The effective χ parameter includes contributions from the peak of the static structure factor

$$2N\chi_{\text{eff}} = 2N\chi_s - N/S^\phi(k^*), \tag{44}$$

taking into account the fact that when the spinodal condition is fulfilled, the inverse concentration contribution of the structure factor does not vanish: the disordered phase is still present and eventually the system undergoes a first-order phase transition.

Analytical intermolecular total correlation functions between like and unlike coarse-grained blocks are predicted by our formalism as a function of chain composition, block size, density, temperature, as well as density and concentration fluctuation screening lengths, in both the real and reciprocal space. Input to our coarse-graining approach is the monomer-level total correlation functions from PRISM [81, 82]. We report here only the expressions for the coarse-grained block–block intermolecular total pair correlation functions in the direct representation

$$h^{\text{bb}}_{\alpha\beta}(r) = h^{\text{bb},\rho}_{\alpha\beta}(r) + \Delta h^{\text{bb},\phi}_{\alpha\beta}(r), \tag{45}$$

where $\alpha, \beta \in \{A, B\}$. Density, $h^{\text{bb},\rho}$ and concentration, $\Delta h^{\text{bb},\phi}$, fluctuation contributions separate, with the density fluctuation contribution given by

$$\begin{aligned} h^{\text{bb},\rho}_{\alpha\beta}(r) = {} & f^2 J^\rho(r, R_{\alpha A\beta A}) \\ & + f(1-f)J^\rho(r, R_{\alpha A\beta B}) + f(1-f)J^\rho(r, R_{\alpha B\beta A}) \\ & + (1-f)^2 J^\rho(r, R_{\alpha B\beta B}), \end{aligned} \tag{46}$$

where $\alpha, \beta \in \{A, B\}$, and $J^\rho(r, R)$ are defined by equation (23). The distance $(R_{\alpha\beta\gamma\delta})^2 = [(R_{g\alpha\beta})^2 + (R_{g\gamma\delta})^2]/2$, where $R_{g\alpha\beta}$ is the average distance of a monomer of type β from the center of mass of the block of type α, as

$$R^2_{g\alpha\beta} = \frac{1}{N_\beta}\sum_{i=1}^{N_\beta}(\vec{r}_{\beta_i} - \vec{R}_{b\alpha})^2. \tag{47}$$

Density fluctuation contributions for each block are formally identical to the coarse-graining expressions obtained for homopolymer melts. This ensures that the block copolymer

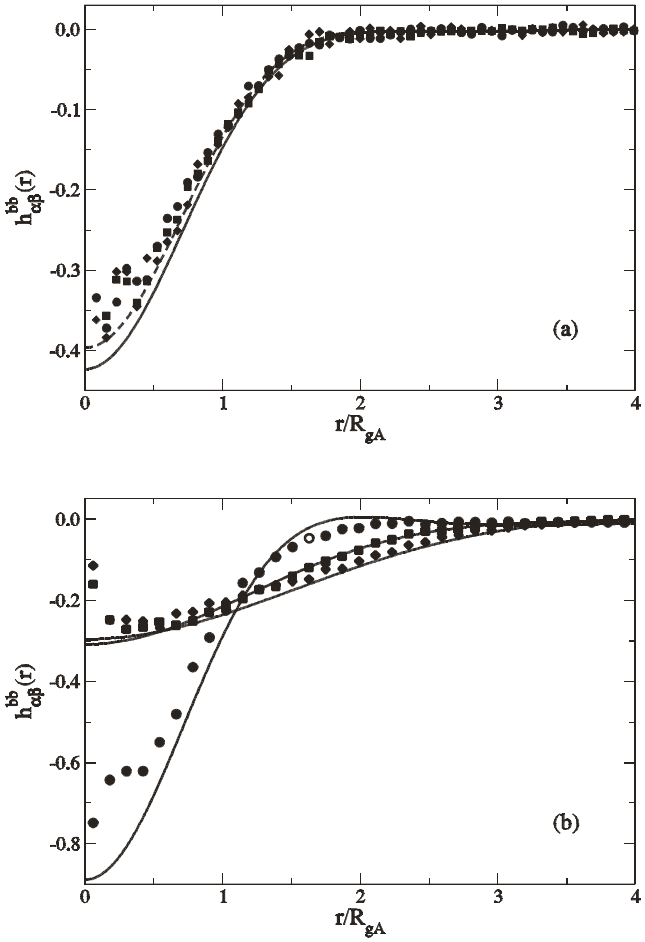

Figure 6. Plot of $h^{\mathrm{bb}}_{\alpha\beta}(r)$. Shown are the theoretical representations (lines) along with data from united atom molecular dynamics simulations (symbols): AA (circles), AB (squares), and BB (diamonds) contributions. Panel (a) is for $f = 0.50$, while panel (b) is for $f = 0.25$. Panel (a) also shows the result from the Debye representation of $\omega^{\mathrm{mm}}_{\alpha\beta}(k)$ (dashed line). Reprinted figure with permission from [31]. Copyright 2007 by the American Physical Society.

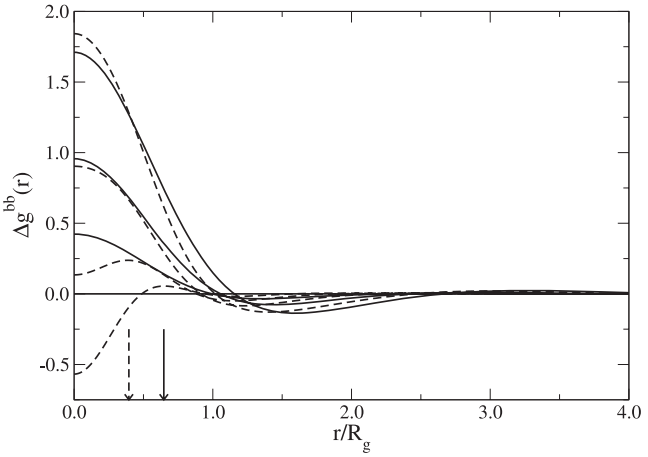

Figure 7. Plot of $\Delta g^{\mathrm{bb}}(r)$ as a function of the distance normalized by the polymer radius of gyration, for various temperatures. From bottom to top: $N\chi_{\mathrm{eff}}/N\chi_{hta,s} \in \{0.0, 0.5, 1.0, 2.0\}$. Shown are the $f = 0.50$ (solid lines) and $f = 0.25$ (dashed lines) cases. The arrows indicate the respective size of A-blocks. Reprinted figure with permission from [31]. Copyright 2007 by the American Physical Society.

formalism correctly recovers the 'homopolymer-like' limit in athermal thermodynamic conditions where concentration fluctuations are suppressed as the system is far from its phase transition.

The contribution due to concentration fluctuations is given by the general equation

$$\Delta h^{bb,\phi}_{\alpha\beta}(r) = \Delta J^{\phi}(r, R_{\alpha A\beta A}) - \Delta J^{\phi}(r, R_{\alpha A\beta B}) - \Delta J^{\phi}(r, R_{\alpha B\beta A}) + \Delta J^{\phi}(r, R_{\alpha B\beta B}), \tag{48}$$

where we define $\Delta J^{\phi}(r, R) = J^{\phi}_{N\chi_{\mathrm{eff}}}(r, R) - J^{\phi}_{0}(r, R)$. In the small r/R_{g} regime of interest here, the concentration fluctuation contribution simplifies, yielding for the auxiliary function $J^{\phi}(r, R)$ the following expression [31]

$$\Delta J^{\phi}(r, R) \approx f^2(1-f)^2\sqrt{\frac{3}{\pi}}\frac{\xi'_{\rho}}{R}\mathrm{e}^{-3r^2/(4R^2)} \times \left(2 + 3\frac{\xi_{\mathrm{c}}^2}{R^2}\right) N\chi_{\mathrm{eff}}. \tag{49}$$

The concentration fluctuation contribution increases with the effective χ parameter. To investigate this effect we define the parameter $\Delta g^{\mathrm{bb}}(r)$, which represents a measure of the physical clustering with temperature of blocks of like species, as

$$\Delta g^{\mathrm{bb}}(r) = g^{\mathrm{bb}}_{AA}(r) + g^{\mathrm{bb}}_{BB}(r) - 2g^{\mathrm{bb}}_{AB}(r). \tag{50}$$

The number of β-type blocks included within a sphere of radius r' from the center of mass of block α, is given by

$$n^{\mathrm{bb}}_{\alpha}(r') = 4\pi\rho_{b\beta}\int_0^{r'} r^2 g^{\mathrm{bb}}_{\alpha\beta}(r)\,\mathrm{d}r + \delta_{\alpha\beta}, \tag{51}$$

with $\alpha, \beta \in \{A, B\}$. Clustering due to concentration fluctuations increases with decreasing temperature, while density fluctuations provide a contribution constant with temperature, which is a consequence of the asymmetry in diblock composition and vanishes for compositionally symmetric diblocks. The scaling with degree of polymerization of the function $\Delta g^{bb,\phi}(r) \propto \sqrt{N}/S(k^*)$ depends on how far the system is from its microphase separation transition. At temperatures higher than the order–disorder temperature ($T \gg T_{\mathrm{ODT}}$), we find that $\Delta g^{bb,\phi}(r) \propto N^{-1/2}$. At the transition temperature ($T \approx T_{\mathrm{ODT}}$), $\Delta g^{bb,\phi}(r) \propto N^{-5/6}$, while in the low-temperature regime ($T \ll T_{\mathrm{ODT}}$), $\Delta g^{bb,\phi}(r) \propto N^{-3/2}$.

As a test of our coarse-graining expressions, we compare theoretical predictions with computer simulation data [33] of homopolymer melts in the athermal ($N\chi_{\mathrm{eff}} = 0$) regime. Because in the high-temperature regime concentration fluctuations are not present, we can test the ability of our description to capture the effect of architectural asymmetry. We consider a diblock copolymer system where chain arms have equal (symmetric, $f = 0.50$), or unequal (asymmetric, $f = 0.25$) size. In both cases, the theory is found to be in agreement, within numerical error, with simulations as figure 6 illustrates. The top panel in the

figure depicts the analytical solution involving both the Padé approximant of the intramolecular structure factors, as well as its Debye approximation, which give comparable agreement with simulations.

In figure 7, we investigate the behavior at the mesoscopic scale of our system as the temperature is modified and the system evolves toward its microphase separation transition. To make contact with the calculations performed in the athermal regime, we investigated a diblock copolymer with a constant, total number of monomers, $N = 96$, identical segment lengths for the two blocks, $\sigma_A = \sigma_B$, and a repulsive Yukawa interaction between unlike monomers. The chain is partitioned, first as a compositionally symmetric diblock, $f = 0.5$ and $N_A = N_B = 48$, and then as a compositionally asymmetric diblock with $f = 0.25$ and $N_A = 24$ and $N_B = 72$. Input to our coarse-graining theory are the values of $S^{\phi}(k^*)$ calculated for these two systems at $N\chi/N\chi_{hta,s} \in \{0.0, 0.5, 1.0, 2.0\}$. These values sample our systems in a range of temperatures that include the athermal limit, $N\chi/N\chi_{hta,s} = 0$, the spinodal temperature, $N\chi/N\chi_{hta,s} = 1$, and the weak segregation limit down to (roughly) the ODT temperature, $N\chi/N\chi_{hta,s} = 2$, calculated following the procedure in [83, 84].

To study the effects of concentration fluctuations at the level of blocks, we focus on the physical clustering of like species as defined in equation (50). In figure 7, $\Delta g^{\mathrm{bb}}(r)$ is shown for the symmetric and asymmetric cases. At athermal conditions concentration fluctuation contributions are absent. Repulsive interactions between unlike monomers are screened and entropic contributions to the free energy are dominant. The symmetric case exhibits no local clustering effects, and the system packs in an entirely random fashion. For the model of diblock copolymer investigated in this study, where the monomer bond lengths for the two blocks are equal ($\sigma_A = \sigma_B$), the two diblocks at high temperature are identical for a compositionally symmetric diblock, i.e. $\Delta g^{\mathrm{bb}}(r) = 0$ for $f = 1/2$. For the asymmetric case, on the other hand, there is an emergence of entropic packing effects arising from the difference in block sizes, yielding a response in $\Delta g^{\mathrm{bb}}(r)$ where AB contacts are favored ($\Delta g^{\mathrm{bb}}(0) < 0$ at high temperature for $f \neq 1/2$).

As the temperature decreases, the formation of self-contacts, AA and BB, becomes energetically favorable, while the system approaches its microphase segregation transition ($\Delta g^{\mathrm{bb}}(0) > 0$). A shallow minimum develops with decreasing temperature, at the distance corresponding to the microdomain size, $r \approx 1.5R_{\mathrm{g}}$ for the symmetric case, since at the interface between domains the number of contacts between unlike species is higher than the number of self-contacts, i.e. $\Delta g^{\mathrm{bb}}(r) < 0$. For compositionally asymmetric diblock copolymers, physical clustering occurs around the minority species, and the minimum is slightly shifted towards the small r region. In both cases, the minimum is smooth and shallow, indicating that there is no sharp transition at the interface between A and B domains, which is a characteristic of the weak segregation regime: fluctuations still partially disorder the liquid, while it becomes increasingly correlated approaching its phase transition.

3. Coarse-graining of dynamical processes

The dynamics of complex fluids develop across many orders of magnitude in time and length scales. Already at the molecular level the dynamics are quite complex. From the local vibrational motion of atoms inside a macromolecule, to center of mass diffusion, more than ten orders of magnitude in time (and space) are comprised. Longer timescales are related to even larger length scales when supermolecular objects are self-assembled. Interestingly enough, formally similar dynamic equations describe the motion of systems that differ by several orders of magnitude in their length scale. For example, at time longer than the internal decorrelation time, the translational dynamics of the center of mass of a molecule follows Brownian motion, which is the same kind of motion performed by a bacterium swimming in a solvent. Both systems follow an overdamped Langevin equation where, however, the parameters in the equation (e.g. the friction coefficient) are quantitatively different. As a second example, the motion of mitochondrial reticulum filaments can be described by a Langevin equation for the dynamics of overdamped particles connected by harmonic springs, which is analogous to the equation of motion of a linear macromolecule, such as polyethylene or a protein [85]. Because the theoretical formalism used to describe the dynamics of these systems on very different length scales is formally identical, the challenge becomes to provide the theoretical tools to determine the values of the parameters entering those equations, from the lower level of coarse-graining. If successful, this way of proceeding could provide us with a complete description of the physics of the system, from the molecular level up to macroscopic scales, across many orders of magnitude.

A key quantity entering the dynamics of coarse-grained systems is the effective potential, which we discussed in the previous sections of this paper. When the system is represented at different levels of coarse-graining, different effective potentials enter the equation of motion, governing its dynamics. For example, the diffusive center of mass motion of a macromolecule, which is uncoupled from its internal conformational transitions, is well represented by the diffusive equation of a soft colloidal particle. The colloidal particle is centered at the position of the molecule center of mass, and interacts with the interpenetrating polymers through the soft-core potential described in the previous sections of this paper. Monomer dynamics, on the other hand, are driven by chain connectivity and the hard-core repulsive potential, which describes the excluded volume interaction between monomers.

The theoretical description of polymer dynamics at the molecular level, utilizes coarse-grained models where effective segments (or monomers) are the fundamental units. Conventional models for polymer dynamics, such as Rouse and Rouse–Zimm theories [46], represent the molecule as a collection of beads, or friction points, connected by an harmonic intramolecular potential, which mimics connectivity. The units in these coarse-grained models correspond to affective particles of the size of one or more monomers, centered on their center of mass position, $\mathbf{r}_i$ with $i = 1, \ldots, N$. Since bond vectors connecting two adjacent beads, $\mathbf{l}_i = \mathbf{r}_{i+1} -$

$\mathbf{r}_i$ are supposed to be uncorrelated, i.e. the polymer chain is completely flexible, with $\langle \mathbf{l}_i \cdot \mathbf{l}_j \rangle = l^2 \delta_{ij}$, the effective segment length has to be larger than or equal to the effective Kuhn segment, which defines the length scale of intramolecular bond correlation.

To treat semiflexible polymers, Bixon and Zwanzig proposed an implemented version of the Rouse model. This is the so-called Optimized Rouse approach, [86] where the local semiflexibility is included by modeling the polymer chain as a freely rotating chain with $\langle \mathbf{l}_i \cdot \mathbf{l}_j \rangle = l^2 g^{|j-i|}$ with $0 \leqslant g \leqslant 1$. If $g = 1$ the theory models the dynamics of a 'Gaussian rod', while if $g = 0$ the Rouse model is recovered. For intermediate values of the stiffness parameter, g, the Optimized Rouse equation describes the dynamics of a chain with local semiflexibility.

Although textbooks introduce Rouse-like theories as 'models', without a derivation from first-principles approaches, these are Langevin equations, i.e. inhomogeneous first-order differential equations, which can be formally derived using projection operation techniques. In general, projection operators are coarse-graining procedures for the *dynamics*, as they allow one to derive a Langevin equation (or equivalently a Fokker–Planck equation) for a coarse-grained model, from the Liouville equation that governs the microscopic level dynamical description [87]. The necessary step in the application of Mori–Zwanzig projection operator technique is the identification, in phase space, of a set of coordinates that represent a group of slowly relaxing particles, and to treat the fast particles in a mean-field way as a heath bath. If two groups of variables have separate timescale of motion, it is possible to project the dynamics of the whole system, as described by the Liouville equation, onto the coordinates of the slow particles, while fast particle are averaged out by the procedure. The resulting Langevin equation is a differential equation, linear in the slow variables, which also contains a memory function contribution describing the history of the system from an 'initial' time to the time t at which the dynamic property is investigated. If a separation of timescales is observed in the complex fluid and if all the slow relevant variables are included in the projection operator, the correction due to the memory function becomes negligible [6]. In this case, the simple inhomogeneous first-order differential equation in the slow variables correctly represents the whole dynamics of the system, while the fast variables enter the equation through the friction coefficient and the random forces.

One of the objectives of a coarse-graining procedure is to provide the value of the different quantities that appear in the Langevin (or, equivalently, the Fokker–Planck) equation. More precisely, one would like to relate the friction coefficient, intramolecular and intermolecular potential, and the correlation of the random forces (drift and diffusion terms of the FPE) to the microscopic molecular description. In the previous sections we described how effective potentials can be obtained as a function of microscopic quantities using liquid state theories. Dynamic quantities, such as friction coefficients, are obtained through the dynamic coarse-graining procedure.

In the conventional model of polymer dynamics, which corresponds to the Rouse equation for polymer melts and the Rouse–Zimm equation for polymers in dilute solutions, the equation of motion is derived by assuming as slow relevant variables, the ensemble of position coordinates of beads, or friction points, of a single molecule. By neglecting the memory function, it is hypothesized that no other relevant slow variables are present in the liquid besides the space coordinates of the 'tagged' molecule. It is clear from the discussion above that Rouse-like theories are a good representation of the dynamics of the system when it is possible to identify one tagged molecule as being slowly moving. As a consequence, it is reasonable to expect Rouse-like equations to describe correctly the dynamics of macromolecules in dilute solutions, where interpolymer interactions are negligible and the solvent is rapidly moving with respect to the solute. The application of Rouse-like approaches for macromolecules in dense solutions (e.g. glassy states, concentrated solutions, and melts) becomes more questionable since the 'solvent' molecules are not expect to relax on timescales shorter than the 'solute', or tagged macromolecule.

In the following sections we present two implementations of the Rouse–Zimm approach, i.e. Langevin equations for macromolecular dynamics, where these considerations are taken into account. In the first example, we investigate the dynamics of polymer melts through an extension of the Rouse approach, which includes the cooperative motion of macromolecular chains interpenetrating with the 'tagged' molecule. The cooperative many-chain dynamics is a function of the intermolecular effective potential of mean force, formally derived through the coarse-graining procedure discussed in the previous sections of this paper. In the second example, we focus on the dynamic of a protein in dilute solutions. This system has no long-lasting intermolecular potential but complex intramolecular interactions, which include chain connectivity, hydrogen bonds, Coulombic forces, and long-range hydrodynamic forces. By means of these two examples, we discuss two limiting cases where novel Langevin equations have been developed, which describe a system with a complex intermolecular potential coupled to a relatively simple intramolecular interaction, i.e. homopolymer melts, and a system with complex intramolecular interactions and simple intermolecular forces, i.e. a protein in dilute solution.

4. Dynamics of a tagged polymer in a liquid of macromolecules: the Langevin equation for cooperative dynamics

On a timescale longer than the ballistic regime but shorter than the longest intramolecular relaxation time, where monomer dynamics crosses over to center of mass motion, Rouse theory predicts that the center of mass mean square displacement follows a linear scaling with time due to Brownian motion, i.e. $\Delta R^2(t) \propto t^\nu$, with $\nu = 1$. Experiments and simulations of polymeric liquids show, however, that the center of mass mean square displacement follows $\Delta R^2(t) \propto t^\nu$, with $\nu < 1$, i.e. a subdiffusive regime, which crosses over to diffusion on the timescale of the longest intramolecular relaxation (see, for example, figure 8) [33, 35, 51]. Analysis of simulation trajectories suggests that the inconsistency between

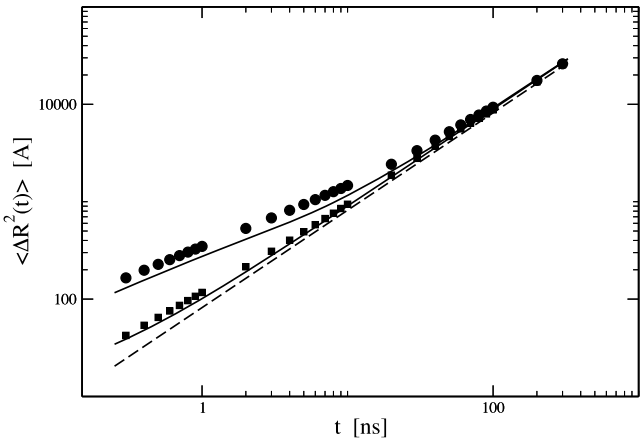

Figure 8. Center of mass and monomer mean square displacements as a function of time for a polyethylene chain. Best fit of the molecular dynamics simulation data for the center of mass (filled squares) and monomer (filled circles) mean square displacements with the many-chain cooperative Langevin equation, equation (52), for polymer melts (solid lines). Also reported is the Rouse center of mass diffusion (dashed line).

single-chain theories and simulations is due to the neglect of intermolecular contributions. This hypothesis is further supported by the observation that similar anomalous diffusion is present in systems of small molecules moving inside polymeric matrices, as well as in polymer solutions above the overlap concentration, but it is not observed in dilute polymer solutions where interpolymer interactions are negligible.

The hypothesis that diffusion of a single tagged chain is uncorrelated with the motion of its surrounding molecules stands on the assumption that there is a separation of timescales between the relaxation of solute and solvent [4, 7]. While this assumption is reasonable for macromolecules in solution of small molecule solvent, where the different size of solvent and solute molecules suggests different timescales of dynamic relaxation, it becomes questionable in polymer melts, because the tagged polymer chain and its surrounding molecules are identical.

Simulations of polymer melts show that the dynamics of a single chain is correlated with the motion of its surrounding molecules for the timescale corresponding to the time necessary for the polymer to escape its own spatial dimension. This decorrelation time is defined as $\tau_{\rm decorr} \approx R_{\rm g}^2/D_{\rm sc}$, with $D_{\rm sc}$ representing the diffusion coefficient of a single chain. By this dynamic mechanism, each polymer chain renews completely its intermolecular contacts, so that if the dynamic is sampled for timescales larger than $\tau_{\rm decorr}$ subsequent steps in the motion of a polymer molecule are uncorrelated, and the molecule follows Brownian motion. The decorrelation time defines the transition from subdiffusive to diffusive motion, and given that it is equivalent to the longest intramolecular relaxation time, there is no separation of timescales between the decay of intramolecular and intermolecular correlations.

In a liquid of macromolecules slow and fast molecules cannot be immediately identified, since all the molecules in the fluid have identical chemical structure and degree of polymerization. In principle each molecule in the liquid should diffuse within the same characteristic correlation time. This state of things leaves little hope for a formally 'rigorous' treatment of the dynamics of such large systems, because the dynamic of every single molecule in the liquid appears to be equally important. This implies the need for a full theoretical treatment for all the molecules, which is an impossible task. However, a careful analysis of computer simulation trajectories for the dynamics of unentangled and entangled polymer melts, shows that while the structure of the liquid is uniform, its dynamics are heterogeneous with interconverting regions of slow and fast dynamics. Because a separation of timescales is observed, it is possible to derive, through projection operator techniques, a Langevin equation for the cooperative dynamics of the *ensemble* of slowly relaxing *semiflexible* polymer chains in the field of fast-moving molecules [88–91]. The resulting Langevin equation describes the dynamics of a segment a, belonging to molecule i and positioned at $\mathbf{r}_a^{(i)}(t)$, as a balance of three different contributions: the intramolecular potential $-\beta^{-1}\ln\{\Psi[\mathbf{r}^{(i)}(t)]\}$, the time-dependent intermolecular potential of mean force $-\beta^{-1}\ln\{g[\mathbf{r}^{(j)}(t), \mathbf{r}^{(k)}(t)]\}$, and the random interactions with the surrounding liquid, given by the projected random force $\mathbf{F}_a^{Q(i)}(t)$. The Langevin equation for cooperative dynamics reads

$$\zeta\frac{\mathrm{d}\mathbf{r}_a^{(i)}(t)}{\mathrm{d}t} = \beta^{-1}\frac{\partial}{\partial\mathbf{r}_a^{(i)}(t)}\ln\left[\prod_{j=1}^{n}\Psi[\mathbf{r}^{(j)}(t)] \times \prod_{k<j}^{n} g[\mathbf{r}^{(j)}(t), \mathbf{r}^{(k)}(t)]\right] + \mathbf{F}_a^{Q(i)}(t), \tag{52}$$

with $\beta = (k_{\rm B}T)^{-1}$. When the time-dependent pair distribution function $g[\mathbf{r}^{(j)}(t), \mathbf{r}^{(k)}(t)] \to 1$, which corresponds to a vanishing potential of mean force $w(r) = -\beta^{-1}\ln g[\mathbf{r}^{(j)}(t), \mathbf{r}^{(k)}(t)] \to 0$, equation (52) recovers the equation of motion (eom) for a single macromolecule in a uniform bath, i.e. the Rouse equation. Instead, if each polymer reduces to a single unit, equation (52) recovers the eom for two interacting colloidal particles, which was derived by Veseley and Posch [92].

The number of correlated molecules is given by the statistical number of polymeric chains in the volume spanned by the tagged chain, which is defined by its radius of gyration, as

$$n(R_{\rm g}) = \left(4\pi\rho\int_0^{R_{\rm g}} r^2[h^{\rm cc}(r)+1]\,\mathrm{d}r\right) - 1 \propto N^{1/2}\rho l_{\rm eff}^3, \tag{53}$$

with $h^{\rm cc}(r)$ the center of mass total correlation function. This number increases with increasing degree of polymerization, N, increasing chain stiffness, $l_{\rm eff}$, and increasing total monomer number density, ρ. In our calculations n is assumed to be an adjustable parameter, whose value is determined by optimizing the agreement of theory against simulation or experimental data.

4.1. Center of mass anomalous diffusion

Once the Gaussian form of the intramolecular and of the intermolecular potentials of mean force are included in

equation (52), the latter can be solved by transformation into normal modes of motion. Dynamics in normal modes decouple into two equations of motion, which represent the relative and the collective contributions, respectively. As a function of the eigenvalues and eigenvectors of the matrices of intramolecular and intermolecular correlation, it is possible to solve all the time correlation functions of interest, which are a linear combination of relative and collective dynamics. Quantities of interest include the statistically averaged, mean square com displacement for the single chain, $\Delta R^2(t) = \langle [R_{\rm com}(t) - R_{\rm com}(0)]^2 \rangle$, where $R_{\rm com}(t)$ is the position coordinate of the polymer com at time t. Relative dynamics are driven by the intermolecular potential, and a single chain experiences a force due to the surrounding polymers, which is approximated by the following equation

$$G(t)R(t) \approx nN\frac{171}{32}\sqrt{\frac{3}{\pi}}\xi_\rho/R_{\rm g}^3 \times \left(1+\sqrt{2}\tilde{\xi}_\rho\right)e^{-75\langle R^2(t)\rangle/(76R_{\rm g}^2)}R(t), \quad (54)$$

with $R(t)$ being a relative, many-chain interpolymer distance. The mean square average distance between a pair of macromolecules is estimated as

$$\langle R^2(t)\rangle \approx n\Delta R^2(t) - 6D_{\rm collective}t, \quad (55)$$

with

$$D_{\rm collective} = D_{\rm sc}(N^{1/2}\rho l_{\rm eff})^{-1}, \quad (56)$$

the cooperative diffusion coefficient representing the dynamics of the com of an ensemble of n interacting molecules, which tends to vanish for systems with a large number of dynamically correlated molecules.

The calculation of the com mean square displacement, and other time correlation functions, has to account for the fact that the intermolecular force of equation (54) depends on the time-dependent intermolecular distance $\langle R^2(t)\rangle$. At a fixed time interval, the equation is solved self-consistently until convergence between calculated and predicted mean square average interpolymer distance is obtained: the procedure is then repeated for small increments of time, $\Delta t = 10^{-2}$ ps. The single-chain com mean square displacement that results from this procedure, exhibits subdiffusive behavior that crosses over to the diffusive regime when $\langle R^2(t)\rangle > R_{\rm g}^2$, i.e. when the molecule diffuses beyond the range of the intermolecular potential of mean force. In the long-time, large-distance, limit polymer dynamics recovers single-chain diffusion.

When sampled at short time intervals, the diffusive dynamics of macromolecules is cooperative due to the effective intermolecular potential. However, as the system configuration is sampled at increasing time intervals, it become less and less correlated with the initial configuration. Two configurations sampled at a time interval longer than the time necessary for a molecule to diffuse outside its volume ($\tau_{\rm decorr}$), or at a distance larger than the range of the potential ($\Delta R^2(t) > R_{\rm g}^2$), are statistically independent and the com dynamics follow Brownian motion.

In figure 8 we show, as an example, the comparison between theoretical predictions and data from UA-MD simulations for a polyethylene chain of $N = 100$ monomers. Input to the theory are the values of $\rho = 0.03242$ sites Å^{-3}, $T = 450$ K, and $l_{\rm eff} = 4.30$ Å from simulations. The single-chain, long-time, diffusion coefficient from UA-MD simulations provides the value of the monomeric friction as $\zeta = k_{\rm B}T/(ND_{\rm sc}) = 0.4179$ dynns cm^{-1}. Figure 8 shows that the theory reproduces quantitatively the com dynamics, including the crossover from subdiffusive to diffusive regimes at $\tau_{\rm decorr} = 18.72$ ns. The number of molecules undergoing cooperative dynamics, $n = 12$, obtained by optimizing the agreement between theory and simulation data, is found to be consistent with its estimated value, as $n \propto N^{1/2}$.

Correlations between scaling exponents, friction, number of correlated molecules, and local flexibility were investigated for a series of homopolymer melts where the number of united atoms in each molecule was kept constant ($N = 96$) while the semiflexibility changed [50], as well as for polymers with identical segment structure and increasing degree of polymerization, N [88–91]. Single-chain center of mass dynamics, as calculated from equation (52), agree with united atom molecular dynamics simulations in the whole range of timescales available, which includes subdiffusive and diffusive, long-time regimes. In general, the slope of the subdiffusive regime, as well as the crossover time are sensitive to the overall polymer spatial dimension, $R_{\rm g}$, which depends on the degree of polymerization, N, as well as on the local bond semiflexibility, $l_{\rm eff}$ [50, 88–91]. For the polymers investigated so far, the extent of anomalous (i.e. subdiffusive) dynamics observed in the plots increases with increasing degree of polymerization and local chain stiffness, in agreement with the theoretical predictions.

4.2. Monomer dynamics

For times shorter than the decorrelation time, Rouse theory predicts for the monomer mean square displacement a crossover from the short-time behavior

$$\Delta r^2(t) = \langle [\mathbf{r}_{N/2}(t) - \mathbf{r}_{N/2}(0)]^2 \rangle = 6Dt(N+1), \quad (57)$$

to the regime

$$\Delta r^2(t) = \sqrt{\frac{12Nl^2Dt}{\pi}}. \quad (58)$$

At $t \approx \tau_{\rm decorr}$ the monomer mean square displacement reduces to the center of mass dynamics and follows Fickian diffusion, $\Delta r^2(t) = 6Dt$.

Experimental data and computer simulations of monomer mean square displacements for a melt of unentangled PE chains show an overall agreement with Rouse dynamics in the long timescale, $t > \tau_{\rm decorr}$. However, in the intermediate regime simulations display a scaling in time stronger than the predicted Rouse behavior, $\Delta r^2(t) \propto t^\nu$ with $\nu > 0.5$ [35, 93]. The observed disagreement is not surprising, since the Rouse model describes the dynamics of an infinitely long and completely flexible polymer. In reality polymer chains have finite size and local semiflexibility, which produce slow, local conformational transitions. More precisely, local flexibility has multiple origins, being related to the complex energy landscape of the polymer, which affects not only the static persistence length, i.e. the energy minima, but also the

possibility of activated barrier crossing, which determines the dynamic aspect of the persistence length [48, 94].

A better agreement between theory and experiments/simulations is obtained once the finite size of the molecule is taken into account, through a matricial representation of the Langevin equation [88–91]. Moreover, the Optimized Rouse approach derived by Bixon and Zwanzig allows one to include local chain semiflexibility by modeling the polymer as a freely rotating chain [86]. For the system illustrated in figure 8, the monomer length is $l_{\text{bond}} = 1.54$ Å and the bond–bond correlation is given by the flexibility parameter $g = 0.74$. Figure 8 shows that our approach, which includes finite size and local semiflexibility, predicts monomer dynamics in good agreement with UA-MD simulations, for the whole range of timescales investigated.

Because the freely jointed model, described by the Rouse approach, does not include local stiffness, it becomes equivalent to a more realistic freely rotating chain model, which includes local stiffness, only for length scales larger than the local persistence length, here $l_{\text{eff}} = 4.30$ Å. This fact explains the crossover to the $t^{0.5}$ exponent, observed in the monomer dynamics of some systems, for length scales larger than the dynamical persistence length but shorter than the molecular radius of gyration, $l_{\text{eff}} < \Delta r < R_{\text{g}}$.

This analysis suggests that intermolecular forces, which are extremely important in modifying the center of mass diffusion, have little effect on the local monomer dynamics, at least for melts of unentangled chains. In fact, the anomalous monomer dynamics observed in experiments and simulations is mostly accounted for by a theoretical model that includes local semiflexibility, while it is not sensitive to the presence of the com intermolecular potential.

5. Coarse-grained dynamics of proteins in dilute solution

The relevant dynamics of a protein in solution span a large range of time and spatial scales from local dynamics, on picosecond timescale, to global conformational transitions and folding, which can happen on timescales of milliseconds and longer. Long-time, large-scale properties depend on the local chemical structure, so that global conformational transitions, intramolecular conformational rearrangements during protein aggregation, and folding dynamics, are functions of the protein primary sequence. In order to predict protein dynamics from its primary sequence, it is necessary to formalize optimized theoretical descriptions that can bridge different orders of magnitude in time and length scales.

Developing a theoretical approach to describe the dynamics of biologically relevant macromolecules has been an ongoing goal in biophysics. The conventional theory for the dynamics of macromolecules in dilute solutions is the Rouse–Zimm approach [46]. This approach has been proven successful in explaining experiments that focus on the dynamics of synthetic macromolecular systems, but it does not provide predictions in quantitative agreement with experiments when protein dynamics are concerned. A reasonable explanation for this observation is that synthetic macromolecules are relatively simpler objects than natural molecules, whose structure and dynamics were optimized by evolution to perform biological functions.

In fact, protein fluctuations are driven by the complex interplay of several forces, which include hydrogen bonding, Coulombic interactions, chain connectivity, and excluded volume forces. Another important contribution to dynamics is give by hydrodynamic interaction forces, which account for the fact that a residue moving in the fluid perturbs the solvent velocity around a second residue, modifying in this way its friction and its dynamics. Hydrodynamic interaction is a slowly decaying, long-ranged force which affects protein long-time dynamics.

Historically, theories for the dynamics of complex macromolecular systems have focused on developing approximated solutions of the memory function correction to the traditional Rouse–Zimm equation [95–97]. We approach the problem from a different perspective, by selecting appropriate slowly relaxing variables, which allows us to minimize the memory function contribution [98]. In our approach Bixon–Zwanzig's Optimized Rouse theory is extended to explicitly include in the hydrodynamic matrix the effect due to residues partially buried inside the molecule. This contribution is particularly important when the dynamics of proteins are concerned, since configurational fluctuations of folded proteins maintain intact their hydrophobic core. Moreover, to account for the complex intramolecular potential, we adopt as an input to the theory structural correlation functions, and equilibrium (temperature and density) and non-equilibrium parameters (friction and viscosity), obtained from atomistic computer simulations, where the solvent is fully described. Stability of the secondary structures, hydrogen bonds, hydrophobic interactions, short-time correlation of solvent molecules to the protein, and more, are implicitly taken into account in the form of the structural correlation functions calculated from simulations, which enter our Langevin Equation for protein dynamics.

From the solution of the equation, time correlation functions are calculated and tested in the short-time regime against simulation and against experiments of x-ray temperature factors and NMR order parameters. The same theory provides theoretical predictions of long-time dynamics, which are tested against experimental data obtained by NMR measurements of longitudinal relaxation time T_1, transverse relaxation T_2, and steady-state nuclear Overhauser effect (NOE). The theory provides predictions of time correlation functions in agreement with simulations and experiments in the short-time regime and with NMR relaxation dynamics in the long-time regime. [98] In this way, one theoretical framework efficiently bridges information from short-to long-time dynamics. The agreement, although not completely quantitative, is remarkable since the test involves independent experimental measurements and no adjustable parameters.

Several theoretical approaches have been developed to correlate NMR relaxation data to models of protein mobility. Of the initial attempts to model NMR relaxation by assuming specific mechanisms of diffusive dynamics [99–101] the most widely accepted is the model-free approach by Lipari and Szabo [102, 103]. In a seminal paper they presented a formally

simple but physically sound theory that maps the decay of the time autocorrelation function for the single bond vector into a linear combination of two uncorrelated dynamic processes. In its simplest form the theory requires three fitting parameters: the local and global correlation times, and a generalized order parameter determined by the weights assigned to the two dynamic processes. The main contribution of the Lipari–Szabo approach is that it allows for an analysis of NMR relaxation data to provide an approximate, although fairly realistic, picture of the local motions of the protein. Later theoretical approaches correlate the measured order parameters to protein entropy [104, 105] and function.

The assumptions in Lipari–Szabo theory are consistent with the dynamics of flexible bonds in a globular protein. For this system, local motions follow two uncorrelated decay processes given by the local bond dynamics and the overall protein tumbling. However, in general, protein dynamics do not obey a simple three parameter scheme and experimental data can be reproduced by the theory only at the expense of introducing a high number of fitting parameters [106–109]. The complexity of the underlying dynamics, even for a simple flexible globular protein, has been made apparent in the recent work by Brüschweiler and co-workers. In the reorientational eigenmode dynamics theory [110, 111] the local reorientation of backbone bonds is obtained from simulations by initially eliminating the overall tumbling motion from MD trajectories. The global dynamic modes are calculated *a posteriori* through a numerical fitting of correlation times. This procedure is repeated until good numerical agreement with the data is achieved. It is clear from this model that, even for globular proteins, the dynamics is a combination of many slow dynamic processes.

Our theory is different from the described approaches because we focus on deriving an equation of motion for protein dynamics that correctly describes a broad range of time regimes, and provides a good prediction of different NMR experiments, (i.e. T_1, T_2 and NOE), x-ray crystallography temperature factors, and computer simulations [98]. We are interested in pursuing this alternative avenue for the following reason: while parameter-dependent models can achieve good agreement with experiments by including an increasing number of adjustable parameters, this is often accomplished at the expense of physical self-consistency and broad predictive power.

The test protein of our approach is the signal transduction protein, CheY. This protein is a member of the superfamily of response regulator proteins, and controls the chemotactic swimming response of motile bacteria. This mechanism of response to stimuli is controlled by a two-component regulatory system, which includes a sensor component, an autophosphorylating protein kinase, and the response regulator CheY. Since two-component regulatory systems are ubiquitous in prokaryotes as well as in low eukaryotes, understanding the role of flexibility and dynamics of the response regulator, CheY, with respect to the general mechanisms of signal transduction is of fundamental scientific interest.

5.1. A Langevin equation for protein dynamics

In our Langevin approach [98], the protein is described as a series of N effective units, or friction points, centered at the α-carbon position of each residue and identified by the vector $\mathbf{r}_i(t)$, with $i = 1, 2, \ldots, N$. Each unit has friction $\zeta_i = \zeta_{i,w} + \zeta_{i,p}$ given by the contribution to the friction due to the area in the residue exposed to the solvent, $\zeta_{i,w} = 6\pi\eta_{\mathrm{w}} r_{i,w}$ and the contribution given by the area screened from the solvent, for example the area exposed to the hydrophobic region of the protein, $\zeta_{i,p} = 6\pi\eta_{\mathrm{p}} r_{i,p}$. Here $r_{i,w}$ ($r_{i,p}$) is the hydrodynamic radius of a spherical bead of surface area equal to the surface exposed (shielded from) the solvent. The internal viscosity of the hydrophobic core of the protein, η_{p}, is assumed to be twice the magnitude of the viscosity of the water solvent, η_{w}. This value is chosen on the physical grounds that residues in the hydrophobic core move in a liquid of hydrophobic particles, similar to the environment of a monomer in a melt of polymer chains.

The time evolution of the space coordinate for unit i obeys the Langevin equation

$$\zeta \frac{\partial \mathbf{r}_i(t)}{\partial t} = -\frac{3k_{\mathrm{B}}T}{l^2} \sum_{j,k=0}^{N-1} H_{i,j} A_{j,k} \mathbf{r}_k(t) + \mathbf{F}_i(t), \tag{59}$$

since the motion of each residue is driven by the balance of forces acting on the residue, which includes the random force, $\mathbf{F}_i(t)$, the viscous force, $\zeta(\partial \mathbf{r}_i(t)/\partial t)$, and the intramolecular force, defined as

$$-\frac{3k_{\mathrm{B}}T}{l^2} \sum_{j,k=0}^{N-1} H_{i,j} A_{j,k} \mathbf{r}_k(t). \tag{60}$$

Here, $\zeta = N^{-1} \sum_{i-0}^{N-1} \zeta_i$ is the average friction coefficient.

The matrix that describes the chain connectivity, $\mathbf{A}$, is coupled to the solvent-mediated hydrodynamic interaction matrix, whose generic element, H_{ij}, describes how the motion of residue i produces instantaneous waves in the solvent, which perturb the velocity of the fluid surrounding a second generic residue j. The random force, due to the collisions of solvent molecules on the residue, obeys the fluctuation-dissipation condition

$$\langle F_{x,i}(t) \cdot F_{y,j}(t') \rangle = 2k_{\mathrm{B}}T\zeta\delta_{xy}\delta_{ij}\delta(t - t'). \tag{61}$$

Here $\mathbf{A}$ is the matrix of intramolecular connectivity which reduces to the Rouse matrix for infinitely long and flexible macromolecules. The connectivity matrix is defined by the product of matrices $A_{i,j} = \sum_{k,p=2}^{N} M_{k,i} U^{-1}_{k,p} M_{p,j}$, where $\mathbf{U}$ is the equilibrium averaged bond correlation matrix

$$U_{k,p} = \frac{\langle \mathbf{l}_k \cdot \mathbf{l}_p \rangle}{l_k l_p}, \tag{62}$$

and $\mathbf{M}$ is the connectivity matrix, with all the elements equal to zero except $M_{0,i} = 1/N$ with $i = 0, \ldots, N-1$, $M_{i,i} = 1$ and $M_{i,i-1} = -1$ with $i = 1, \ldots, N-1$. The $\mathbf{U}$ matrix for our protein is defined by the statistical averages calculated from simulation trajectories. In this way the intramolecular

potential, $V_{i,j} = 3k_BTl^{-2}\mathbf{r}_i A_{i,j}\mathbf{r}_j$ implicitly contains all the relevant contributions of intramolecular origin due to the complex force field that drives protein motion.

A new feature of our approach is the definition of the hydrodynamic interaction matrix,

$$H_{i,j} = \frac{\zeta}{\zeta_i}\delta_{i,j} + (1-\delta_{i,j})\frac{\zeta_w}{6\pi\eta_w}\left\langle\frac{1}{R_{i,j}}\right\rangle, \tag{63}$$

which in the new form of equation (63) properly accounts for residues partially screened from the solvent. Here, $\zeta_w = N^{-1}\sum_{i-0}^{N-1}\zeta_{i,w}$ is the average friction coefficient for the area exposed to the solvent. In the conventional definition of the hydrodynamic interaction, i.e. the Rouse–Zimm approach, residues are supposed to be statistically fully exposed to solvent. This is a good approximation for synthetic polymers in good and theta solvents; however, for folded proteins the use of the conventional approach leads to unphysical results. The statistically averaged inverse distances, entering the matrix **H**, are calculated from the trajectory of the MD simulation of the protein in solution.

Equation (59) represents a set of N coupled equations of motion, which decouple by Fourier transform into normal mode coordinates. Eigenvalues and eigenvectors of the matrix product **HA** allow for the solution of any time correlation function of interest, including functions that decay on a timescale longer than the range of the simulation. The quality of agreement we obtain between our approach and available experimental data supports the validity of our description [98].

5.2. Test of the theory against experimental data of NMR relaxation

The time correlation function of interest for the study of protein dynamics is the autocorrelation function $P_2^i(t)$, which is the second-order Legendre polynomial of the cosine of the angle spanned by the reorientation of the bond vector i during time t. The Fourier transform of $P_2^i(t)$ is the spectral density, which determines the relaxation times measured in NMR experiments, such as the nuclear Overhauser effect (NOE), the spin–lattice relaxation time (T_1), and the spin–spin relaxation time (T_2) [114–116].

Perico and Guenza [112, 113] have shown that for a macromolecule, the autocorrelation function $P_2^i(t)$ is simply expressed as a function of the time correlation function $M_1^i(t)$ as

$$P_2^i(t) = 1 - 3\left[x^2 - \frac{\pi}{2}x^3\left(1 - \frac{2}{\pi}\arctan x\right)\right], \tag{64}$$

with

$$x = \left[1 - \left(M_1^i(t)\right)^2\right]^{1/2} \Big/ M_1^i(t). \tag{65}$$

The time correlation function $M_1^i(t)$ is defined as a function of eigenvalues, λ_a, and eigenvectors, $Q_{i,a}$, of the matrix product **HA** and the eigenvalues, μ_a of the matrix **A**, according to

$$M_1^i(t) = \frac{\langle\mathbf{l}_i(t)\cdot\mathbf{l}_i(0)\rangle}{\langle l_i(t)\rangle\langle l_i(0)\rangle} = \sum_{a=0}^{N-1}\left(Q_{i+1,a} - Q_{i,a}\right)^2\mu_a^{-1}\exp\{-\sigma\lambda_a t\}, \tag{66}$$

and $\sigma = 3k_BT/(l^2\zeta)$.

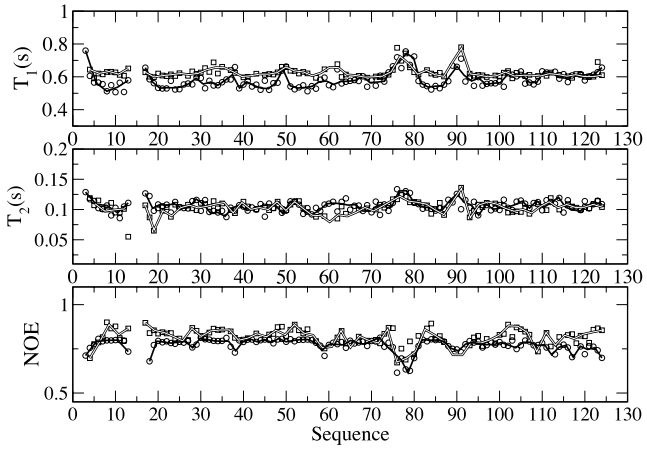

Figure 9. Comparison between theoretical predictions (circles) and experiments (squares) of spin–lattice relaxation time (T_1), spin–spin relaxation time (T_2), and NOE of *Escherichia coli* signal regulator protein CheY. Splines interpolate theory (black lines) and experiments (white lines). Reprinted with permission from [98]. Copyright 2007. Biophysical Society.

In figure 9 we show a comparison between theoretical predictions and experiments for T_1, T_2, and NOE of *Escherichia coli* CheY. For all of the residues, we find that the theory reproduces well the experimentally observed trend of fast and slow relaxation. Notice that the slow relaxation processes mentioned here do not include slow exchange processes, which cannot be predicted by our theory in its present stage of development. The baseline in the data represents the overall protein rotation, which relates to the protein long-time dynamics and depends on the model for hydrodynamic interaction. Peaks in the spin–lattice relaxation indicate local flexibility and fast relaxation. Both theory and experiments show an enhanced flexibility in regions of the protein corresponding to the $\alpha_2 - \beta_3$ loop (47–52), the $\beta_4 - \alpha_4$ loop (87–92), and the turn including bonds 76–80. For purposes of visual clarity, we have omitted from figure 9 the trivial relaxation of the bonds at the two ends of the protein. For those segments, both theory and experiments show enhanced flexibility and fast dynamics due to the lack of connectivity, so that NMR relaxation times largely exceed the range depicted in the figure.

The relatively good agreement between theory and three independent experimental data sets is encouraging, especially in light of the fact that more than 350 data points are described without the need for adjustable parameters. In conclusion, the quality of agreement obtained in this study shows that simulations, theory, and experiments are largely compatible in providing consistent information on the physics of the system.

5.3. NMR order parameters

Through the direct modeling of NMR relaxation data using the Lipari–Szabo theory, a commonly extracted quantity is the order parameter $S_i^2 = P_2^i(\Delta t)$ with $0 < \Delta t < \tau_R$ and τ_R the protein orientational correlation time, i.e. the time of global molecular rotation. For times short in comparison to the

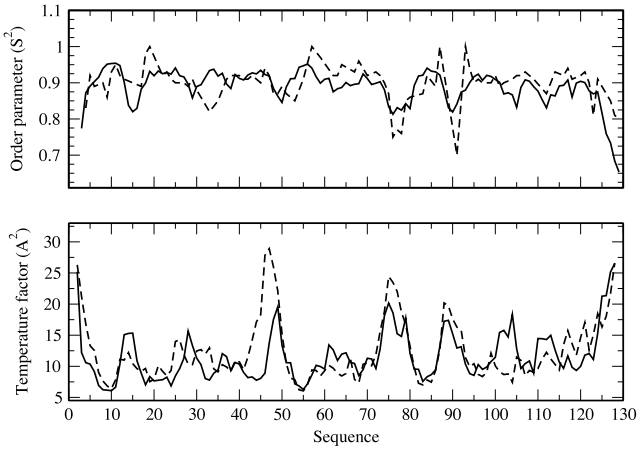

Figure 10. Comparison between theoretical predictions (full line) and experiments (dashed line) of NMR order parameter (top panel) and x-ray temperature factors (bottom panel) of *Escherichia coli* signal regulator protein CheY. Reprinted with permission from [98]. Copyright 2007, Biophysical Society.

relaxation of the orientational time correlation function, $P_2^i(t)$, the bond reorientation can appear restricted to fluctuations around a specific angle. This angle could be similar to that in the proteins native conformation, suggesting that the bond is part of a rigid local structure and $S_i^2 = 1$. Alternatively, the angle could strongly differ from that of the native structure if the bond is flexible, i.e., $S_i^2 \leqslant 0.7$. In figure 10 (top panel), we directly compare our theoretically predicted order parameters with the corresponding values extracted from experimental NMR data using the Lipari–Szabo theory. Several bonds in CheY cannot be modeled and experimental values are available only for 90 of the 129 residues. We chose the sampling time interval for the theoretical data by optimizing the agreement between the orientational correlation function for the first bond along the protein sequence and its corresponding experimental value.

In general, order parameters extracted from NMR data have sharp peaks and fast transitions from completely immobile to strongly mobile residues, along the primary sequence, while the theory exhibits a smoother behavior. This could be due to the fact that data from experiments are obtained by representing the overall decay of the function as a two-steps relaxation, which is often an unrealistic approximation. On the other hand, the theory contains contributions from N modes of relaxation.

Overall, the agreement between our theory and the experimental data is good for the entire primary sequence. Both theory and experiments show several regions with significant loss of orientation, including the two ends of the protein, the $\alpha_2 - \beta_3$ loop (residues 47–52), the $\beta_4 - \alpha_4$ loop (residues 87–92), and the turn (residues 76–80), consistent with the relaxation data discussed earlier.

5.4. X-ray temperature factors

As a second test of the theory in the short-time regime, we compare its predictions of temperature factors against the corresponding experimental values obtained from high resolution x-ray crystallography of *Escherichia Coli* CheY by Volz and Matsumura [117]. The theoretical value of the temperature factors for bond i, B_i, is a function of the residue mean square fluctuation about its equilibrium position, and is a simple function of eigenvalues, λ_a, and eigenvectors, $Q_{i,a}$, of the matrix product **HA** and the eigenvalues, μ_a of the matrix **A**, as

$$B_i = \frac{8\pi^2}{3}\langle[\mathbf{R}_i(t) - \mathbf{R}_i(0)]^2\rangle = \frac{16\pi^2 l^2}{3}\sum_{a=0}^{N-1}\frac{(Q_{i+1,a})^2}{\mu_a}[1 - \exp(-\sigma\lambda_a t)], \quad (67)$$

where $\sigma = 3k_B T/(l^2\zeta)$. If the equation of motion correctly represents the dynamics of the protein under consideration, the same equation should also provide a good representation of short-time fluctuations as measured by temperature factors.

Because the time interval of the fluctuations measured by x-ray experiments is not known, we assume in our calculations a time interval of $\Delta t = 3.5$ ps, which provides the best agreement for the baseline between our predictions and the experimental data. The adopted value of 3.5 ps is consistent with an estimated value. Furthermore, we observe that differences in Δt on the order of 0.5 ps do not significantly change the quality of the agreement between theory and experiment. Figure 10 (bottom panel) shows that both experiment and theory present similar regions of enhanced short-time fluctuations along the protein primary structure. Most of these regions correspond to flexible loops. The agreement between theory and experiment is good, and comparable to the agreement obtained using other theoretical models such as the Gaussian network models pioneered by Bahar, Erman, Jernigan, Tirion, and co-workers [118–120]. A notable factor that affects the precision of the experimental data is the presence of intermolecular constraints due to crystal packing. Intermolecular constraints, which are absent in physiological conditions and are not included in our approach, suppress the amplitude of local fluctuations, and could be responsible for the lack of mobility observed, for example, in the region defined by residues 100–105. In summary, figures 9 and 10 illustrate the utility of a general approach for protein dynamics, which describes in a unified theoretical framework data obtained from independent measurements and different experimental techniques.

6. Summary and conclusions

Because the dynamics of macromolecules develop across many orders of magnitude in time and length scale, experiments and simulations can provide information only on a restricted range of those properties. Therefore, theoretical approaches that describe structure and dynamics of polymer liquids become an indispensable tool because they allow to connect in an unified physical picture the different pieces of information obtained experimentally and from simulations. The development of such theoretical models is, however, quite challenging, given the complexity of the systems investigated. Recently, one main focus in polymer physics has been the development of

novel theoretical techniques, which involve coarse-graining procedures. For example, structural coarse-graining allow one to investigate a system at different levels of detail, through mesoscale simulations, and then combine, in a multiscale procedure, the information obtained into a complete physical picture.

In this work we reviewed recent developments in the theory of structural and dynamic coarse-graining of complex macromolecular liquids. The approaches presented are first-principles ones, as opposed to phenomenological, since they use conventional tools of equilibrium and non-equilibrium statistical mechanics. Although this review focuses mostly on recent research developments by our group, the theory is introduced in the context of the larger framework of the existing literature. When possible, the theory is compared against simulations and against experimental data to provide support to the new hypotheses introduced.

More specifically, this review discusses new analytical methods to coarse-grain the structure of macromolecular liquids of increasing molecular complexity, such as homopolymer and block copolymer liquids and their mixtures. Effective pair potentials acting between coarse-grained units are calculated using liquid state theory. Those potentials are found to provide a reliable representation of the thermodynamic of the system. Moreover, potentials of mean force, so derived, are input to equations of motion of macromolecular dynamics.

Langevin equations are derived by applying projection operator techniques to the Liouville equation, using the well-established coarse-graining procedure for liquid dynamics. As an example, we introduced an equation of motion for the cooperative dynamics of a group of interacting polymers in a liquid, where interpolymer interactions are responsible for the anomalous center of mass diffusion observed in simulations and scattering experiments. Next, we presented a Langevin equation for the dynamics of proteins in dilute solution, which includes a novel form of the hydrodynamic interaction matrix, and we calculated time correlation functions that are measured in NMR and x-ray experiments. The validity of the discussed theoretical approaches is supported by the good agreement observed as theoretical predictions are compared against available simulation and experimental data.

Acknowledgments

My thanks go to my mentors, Angelo Perico, who first introduced me to the physics of macromolecules, Karl Freed, and Ken Schweizer who gave me the opportunity to learn more about statistical mechanics and the theory of complex fluids: many of the ideas that we developed together were seeds for the new work discussed here. I am also indebted to the members of my group, without whom this research could not have been accomplished: Jenelle Bray, Esther Caballero-Manrique, Todd Crum, Pallavi Debnath, Maria Nemirovskaya, Edward Sambriski, and Galina Yatsenko. Many colleagues have supported this work with discussions and collaborations. I wish to thank them for their long-standing support, in particular Rick Dahlquist, Gary Grest, and Andrew Marcus. Acknowledgement is made to the donors of the Petroleum Research Fund, administrated by the ACS, for partial support of this research. This work has been supported over the years by the National Science Foundation under grants: DMR-9971687, DMR-0207949, and DMR-0509808.

References

[1] Barrat J-L and Hansen J-P 2003 *Basic Concepts for Simple and Complex Liquids* (Cambridge: Cambridge University Press)
[2] Larson R G 1999 *The Structure and Rheology of Complex Fluids* (New York: Oxford University Press)
[3] Witten T A and Pincus P A 2004 *Structured Fluids* (New York: Oxford University Press)
[4] Hansen J-P and McDonald I R 1991 *Theory of Simple Liquids* (London: Academic)
[5] McQuarrie D A 1976 *Statistical Mechanics* (New York: Harper Collins)
[6] Zwanzig R 2001 *Nonequilibrium Statistical Mechanics* (New York: Oxford University Press)
[7] Balucani U and Zoppi M 1994 *Dynamics of the Liquid State* (Oxford: Oxford Science Publications)
[8] Mazo R M 2002 *Brownian Motion, Fluctuations, Dynamics and Applications* (Oxford: Oxford Science Publications)
[9] Müller M, Kastov K and Schick M 2006 *Phys. Rep.* **434** 113
[10] Nielsen S O, Lopez C F, Srinivas G and Klein M L 2004 *J. Phys.: Condens. Matter* **16** R481
[11] Alder B J 1964 *Phys. Rev. Lett.* **12** 317
[12] Rice S A and Grey P 1965 *Statistical Mechanics of Simple Liquids* (New York: Interscience)
[13] Kremer K and Grest G 1990 *J. Chem. Phys.* **92** 5057
[14] Uhlherr A, Doxastakis M, Mavrantzas V G, Theodorou D N, Leak S J, Adam N E and Nyberg P E 2002 *Europhys. Lett.* **57** 506
[15] Akkermans R L C and Briels W J 2000 *J. Chem. Phys.* **113** 6409
[16] Akkermans R L C and Briels W J 2001 *J. Chem. Phys.* **114** 1020
[17] Karttunen M, Vattualainen I and Lukkarinen A (ed) 2004 *Novel Methods in Soft Matter Simulations* (*Springer Lect. Notes Phys.* vol 640) (Berlin: Springer)
[18] Everaers R, Sukumaran S K, Grest G S, Svaneborg C, Sivasubramanian A and Kremer K 2004 *Science* **303** 823
[19] Sukumaran S K, Grest G S, Kremer K and Everaers R 2005 *J. Polym. Sci.* B **43** 917
[20] Ganesan V and Fredrickson G H 2001 *Europhys. Lett.* **55** 814
[21] Barbieri A, Campani E, Capaccioli S and Leporini D 2004 *J. Chem. Phys.* **120** 437
[22] Spyriouni T, Tzoumanekas C, Theodorou D, Müller-Plathe F and Milano G 2007 *Macromolecules* **40** 3876
[23] Louis A A 2002 *J. Phys.: Condens. Matter* **14** 9187
[24] Schweizer K S and Curro J G 1994 *Adv. Polym. Sci.* **116** 319
[25] Schweizer K S and Curro J G 1997 *Adv. Chem. Phys.* **98** 1
[26] Yatsenko G, Sambriski E J, Nemirovskaya M A and Guenza M G 2004 *Phys. Rev. Lett.* **93** 257803
[27] Sambriski E J, Yatsenko G, Nemirovskaya M A and Guenza M G 2006 *J. Chem. Phys.* **125** 234902
[28] Soper A K 1996 *Chem. Phys.* **202** 295
[29] Reatto L, Levesque D and Weis J J 1986 *Phys. Rev.* A **33** 3451
[30] Evans R A 1990 *Mol. Simul.* **4** 409
[31] Sambriski E J and Guenza M G 2007 *Phys. Rev.* E **76** 051801
[32] Heine D, Wu D T, Curro J G and Grest G S 2003 *J. Chem. Phys.* **118** 914
[33] Jaramillo E, Wu D T, Grest G S and Curro J G 2004 *J. Chem. Phys.* **120** 8883
[34] Baschnagel J and Varnik F 2005 *J. Phys.: Condens. Matter* **17** R851

[35] Paul W, Yoon D Y and Smith G D 1995 *J. Chem. Phys.* **103** 1702
[36] Binder K 2002 *Comput. Phys. Commun.* **147** 22
[37] Dautenhahn J and Hall C 1994 *Macromolecules* **27** 5399
[38] Murat M and Kremer K 1998 *J. Chem. Phys.* **108** 4340
[39] Eurich F and Maass P 2001 *J. Chem. Phys.* **114** 7655
[40] Flory P J and Krigbaum W R 1950 *J. Chem. Phys.* **18** 1086
[41] Grosberg A Y, Khalatur P G and Khokhlov A R 1982 *Makromol. Chem.* **3** 709
[42] Krüger B, Schäfer L and Baumgärtner A 1989 *J. Physique* **50** 319
[43] Hansen J-P, Addison C I and Louis A A 2005 *J. Phys.: Condens. Matter* **17** S3185 and references therein
[44] Stillinger F H and Weber T A 1980 *Phys. Rev.* B **22** 3790 and references therein
[45] Krakoviack V, Hansen J-P and Louis A A 2002 *Europhys. Lett.* **58** 53
[46] Doi M and Edwards S F 1986 *The Theory of Polymer Dynamics* (Oxford: Oxford University Press)
[47] Yamakawa H 1971 *Modern Theory of Polymer Solutions* (New York: Harper and Row)
[48] de Gennes P-G 1979 *Scaling Concepts in Polymer Physics* (Ithaca, NY: Cornell University Press)
[49] Fredrickson G 2006 *The Equilibrium Theory of Inhomogeneous Polymers* (New York: Oxford University Press)
[50] Sambriski E J, Yatsenko G, Nemirovskaya M A and Guenza M G 2007 *J. Phys.: Condens. Matter* **19** 205115
[51] Mondello M and Grest G S 1997 *J. Chem. Phys.* **106** 9327
[52] Sambriski E J and Guenza M G 2007 unpublished
[53] Balsara N 1996 *Physical Properties of Polymers Handbook* ed J E Mark (Woodbury, NY: AIP)
[54] Olabisi O, Robeson L M and Shaw M T 1979 *Polymer–Polymer Miscibility* (New York: Academic)
[55] Muller M 1999 *Macromol. Theory Simul.* **8** 343 and citations therein
[56] Clancy T C, Putz M, Weinhold J D, Curro J G and Mattice W L 2000 *Macromolecules* **33** 9452
[57] Faller R 2004 *Macromolecules* **37** 1095
[58] Dudowicz J and Freed K F 1991 *Macromolecules* **24** 5076
[59] Dudowicz J and Freed K F 1991 *Macromolecules* **24** 5112
[60] Dudowicz J, Freed K F and Douglas J F 2002 *Phys. Rev. Lett.* **88** 095503
[61] Yatsenko G, Sambriski E J and Guenza M G 2005 *J. Chem. Phys.* **122** 054907
[62] Krishnamoorti R, Graessley W W, Fetters L J, Garner R T and Lohse D J 1995 *Macromolecules* **28** 1252
[63] Bhatia A B and Thornton D E 1970 *Phys. Rev.* B **2** 3004
[64] Kirkwood J G and Buff F P 1951 *J. Chem. Phys.* **19** 774
[65] Sambriski E J and Guenza M G 2008 unpublished
[66] Hamley I W (ed) 2004 *Developments in Block Copolymer Science and Technology* (New Jersey: Wiley, Hoboken)
[67] Balsara N P and Park M J 2006 *J. Polym. Sci.* B **44** 3429
[68] Tsori Y and Andelman D 2006 *J. Polym. Sci.* B **44** 2725
[69] Reith D, Pütz M and Müller-Plathe F 2003 *J. Comput. Chem.* **24** 1624
[70] Li X, Kou D, Rao S and Liang H 2006 *J. Chem. Phys.* **124** 204909
[71] Pierleoni C, Addison C I, Hansen J P and Krakoviack V 2006 *Phys. Rev. Lett.* **96** 128302
[72] Addison C I, Hansen J P, Krakoviack V and Louis A A 2005 *Mol. Phys.* **103** 3045
[73] Hansen J P and Pearson C J 2006 *Mol. Phys.* **104** 3389
[74] David E F and Schweizer K S 1994 *J. Chem. Phys.* **100** 7767
[75] David E F and Schweizer K S 1994 *J. Chem. Phys.* **100** 7784
[76] Leibler L 1980 *Macromolecules* **13** 1602
[77] Matsen M W and Bates F S 1996 *Macromolecules* **29** 1091
[78] Matsen M W and Schick M 1996 *Curr. Opin. Colloid Interface Sci.* **1** 329
[79] Fredrickson G H and Helfand E 1987 *J. Chem. Phys.* **87** 697
[80] Brazovskii S A 1975 *Sov. Phys.—JETP* **41** 85
[81] Guenza M, Tang H and Schweizer K S 1998 *J. Chem. Phys.* **108** 1257
[82] Guenza M and Schweizer K S 1998 *J. Chem. Phys.* **108** 1271
[83] Guenza M and Schweizer K S 1997 *J. Chem. Phys.* **106** 7391
[84] Guenza M and Schweizer K S 1997 *Macromolecules* **30** 4205
[85] Knowles M K, Guenza M G, Capaldi R A and Marcus A H 2002 *Proc. Natl Acad. Sci. USA* **99** 14777
[86] Bixon M and Zwanzig R 1978 *J. Chem. Phys.* **69** 1896
[87] Grabert H 1982 *Projection Operator Techniques in Nonequilibrium Statistical Mechanics* (Berlin: Springer)
[88] Guenza M G 1999 *J. Chem. Phys.* **110** 7574
[89] Guenza M 2002 *Phys. Rev. Lett.* **88** 025901
[90] Guenza M G 2002 *Macromolecules* **35** 2714
[91] Guenza M G 2003 *J. Chem. Phys.* **119** 7568
[92] Veseley F J and Posch H A 1988 *Mol. Phys.* **64** 97
[93] Padding J T and Briels W J 2001 *J. Chem. Phys.* **114** 8685
[94] Ding Y and Sokolov A P 2004 *J. Polym. Sci.* B **42** 3505
[95] Guenza M and Freed K F 1996 *J. Chem. Phys.* **105** 3823
[96] La Penna G, Perico A and Genest D 2000 *J. Biomol. Struct. Dyn.* **17** 673
[97] Giachetti A, La Penna G, Perico A and Banci L 2004 *Biophys. J.* **87** 498
[98] Caballero-Manrique E, Bray J K, Deutschman W A, Dahlquist F W and Guenza M G 2007 *Biophys. J.* **93** 4128
[99] Woessner D E 1962 *J. Chem. Phys.* **36** 1
[100] Wallach D 1967 *J. Chem. Phys.* **47** 5258
[101] Bremi T, Brüschweiler R and Ernst R R 1997 *J. Am. Chem. Soc.* **119** 4272
[102] Lipari G and Szabo A 1982 *J. Am. Chem. Soc.* **104** 4546
[103] Lipari G and Szabo A 1982 *J. Am. Chem. Soc.* **104** 4559
[104] Massi F and Palmer A G III 2003 *J. Am. Chem. Soc.* **125** 11158
[105] Yang D W, Mok Y K, Forman-Kay J D, Farrow N A and Kay L E 1997 *J. Mol. Biol.* **272** 790
[106] Clore G M, Szabo A, Bax A, Kay L E, Driscoll P C and Gronenborn A M 1990 *J. Am. Chem. Soc.* **112** 4989
[107] Vugmeyster L, Raleigh D P, Palmer A G III and Vugmeister B E 2003 *J. Am. Chem. Soc.* **125** 8400
[108] Chang S-L, Szabo A and Tjandra N 2003 *J. Am. Chem. Soc.* **125** 11379
[109] Baber J L, Szabo A and Tjandra N 2001 *J. Am. Chem. Soc.* **123** 3953
[110] Prompers J J and Brüschweiler R 2001 *J. Am. Chem. Soc.* **123** 7305
[111] Prompers J J and Brüschweiler R 2002 *J. Am. Chem. Soc.* **124** 4522
[112] Perico A and Guenza M G 1985 *J. Chem. Phys.* **83** 3103
[113] Perico A and Guenza M G 1986 *J. Chem. Phys.* **84** 510
[114] Bloch F 1956 *Phys. Rev.* **102** 104
[115] Redfield A G 1957 *IBM J. Res. Dev.* **1** 19
[116] Redfield A G 1965 *Adv. Magn. Reson.* **1** 1
[117] Volz K and Matsumura P 1991 *J. Biol. Chem.* **266** 15511
[118] Bahar I, Atligan A R, Demirel M C and Erman B 1998 *Phys. Rev. Lett.* **80** 2733
[119] Bahar I, Erman B, Haliloglu T and Jernigan R L 1997 *Biochemistry* **36** 13512
[120] Tirion M M 1996 *Phys. Rev. Lett.* **77** 1905